Geology of the Sinwa Creek area, northwest BC (104K/14)

Mitchell G. Mihalynuk[1, a], Alexandre Zagorevski[2], Joseph M. English[3], Michael J. Orchard[2], Anna K. Bidgood[4], Nancy Joyce[2], and Richard M. Friedman[5]

[1] British Columbia Geological Survey, Ministry of Energy and Mines, Victoria, BC, V8W 9N3
[2] Geological Survey of Canada, Ottawa, ON, K1A 0E8
[3] Geoscience Consultant, Clonskeagh, Dublin, D14, Ireland
[4] Department of Earth Sciences, University of Oxford, Oxford, United Kingdom, OX1 3AN
[5] Pacific Centre for Geochemical and Isotopic Research, University of British Columbia, Vancouver, BC, V6T 1Z4
[a] corresponding author: Mitch.Mihalynuk@gov.bc.ca

Recommended citation: Mihalynuk, M.G., Zagorevski, A., English, J.M., Orchard, M.J., Bidgood, A.K., Joyce, N., and Friedman, R.M., 2017. Geology of the Sinwa Creek area, northwest BC (104K/14). In: Geological Fieldwork 2016, British Columbia Ministry of Energy and Mines, British Columbia Geological Survey Paper 2017-1, pp. 153-178.

Abstract

Stikine terrane is one of the largest crustal blocks in the Cordillera, measuring more than 1100 km long and 250 km wide. In northern British Columbia it is well known for its large porphyry Cu-Au ±Mo-Ag deposits. Stikine terrane tapers northward, replaced by a broadening wedge of oceanic crustal rocks of the Cache Creek terrane, interpreted to have overthrust Stikine terrane reducing its exposed width to ~10 km at 60°N. This overthrust region is where Triassic-Jurassic magmatic belts with known porphyry deposits disappear, and it is mostly underlain by Triassic-Jurassic arc-derived clastic rocks of the Whitehorse trough. Overthrusting has traditionally been attributed to the northwest-trending King Salmon fault, which carries conspicuous Late Norian Sinwa Formation limestone in its hanging wall. On many terrane maps, the Sinwa Formation marks the western margin of the oceanic Cache Creek terrane. However, clast provenance, biochronology, conodont fossil fauna, and sedimentary facies carried by the King Salmon fault are inconsistent with this interpretation. Instead, these data suggest that rocks in the hangingwall of the King Salmon fault were deposited in the Triassic forearc of the Stikine terrane, isolated from the subducting Cache Creek oceanic lithosphere by an intervening trench. Thus, the King Salmon fault is not a terrane boundary, and although regionally important, it is but one of several faults that carry Sinwa Formation limestone. Complicating this simple tectonic picture are detrital zircons from one sample collected in the footwall of the King Salmon fault. They form a nearly unimodal population with a main peak at 242 Ma, an age unknown in Stikinia but common within volcanic and plutonic rocks of the Kutcho-Sitlika-Venables arc, which have historically been included in the Cache Creek terrane. If this provenance link is correct, it supports the Kutcho-Sitlika-Venables arc as a separate terrane, distinct from the Cache Creek, and juxtaposed with the Stikine forearc before the Bajocian (~173 Ma) juxtaposition of Cache Creek terrane. King Salmon and adjacent fault panels carry steep northeast plunging folds having southeast-dipping axial surfaces, consistent with a top to the north component of motion (or sinistral if originally steep) that may be related to a phase of deformation during latest Triassic Kutcho-Sitlika-Venables arc collision.

Keywords: Sinwa Formation, Stuhini Group, Lewes River Group, Whitehorse Trough, Cache Creek terrane, Stikine terrane, Kutcho-Sitlika-Venables arc, Whitehorse trough fold and thrust belt

1. Introduction

A prolific belt of porphyry copper deposits tracks northward in British Columbia to the Sheslay River area where it seems to disappear (Fig. 1). South of this latitude (~58.5°N) the Late Triassic – Early Jurassic Stuhini and Hazelton volcanic arcs that spawned the prorphyry deposits are coextensive and have east-west dimensions of ~250 km. Between 58.5°N and the BC-Yukon border (60°N), the map extent of the Triassic arc thins to less than 10 km, and Early Jurassic volcanic rocks are unknown. In their place is a northward-widening wedge of oceanic crustal and accretionary complex rocks of the Cache Creek terrane and an intervening belt of marine sedimentary strata known as the Whitehorse trough (Wheeler, 1961; Fig. 1). At the southern apex of the wedge, Cache Creek and Whitehorse trough rocks are structurally interleaved (Monger and Thorstad, 1978) leading to inclusion of the Whitehorse trough with the Cache Creek terrane (Wheeler and McFeely, 1991; Gabrielse et al., 1992). Thus defined, the Cache Creek terrane is bounded to the west by a belt of Late Triassic carbonate rocks called the Sinwa Formation, which are carried by a regional structure, the King Salmon fault. In the Sinwa Creek area, the King Salmon fault is mainly a southwest verging thrust (Monger, 1975; Souther, 1971). Just how this crustal-scale thrust has interacted with the metalliferous Triassic-Jurassic arcs is critically important to tracking the porphyry belts farther north. Did the thrust cut off the Triassic and younger arc edifices, or did it tectonically bury the mineralized arc? If buried, do windows exist in the thrust sheet through which the underlying arc may be accessed, or nearly so? Or, is the thrust coincident with a northward arc submergence and regionally diminished arc edifices, as might be inherited from Mesozoic trench geometry.

In 2015, we conducted regional mapping in the Sinwa Creek map area, where the King Salmon fault is well exposed and where the Sinwa Formation was first defined (Fig. 2). Here

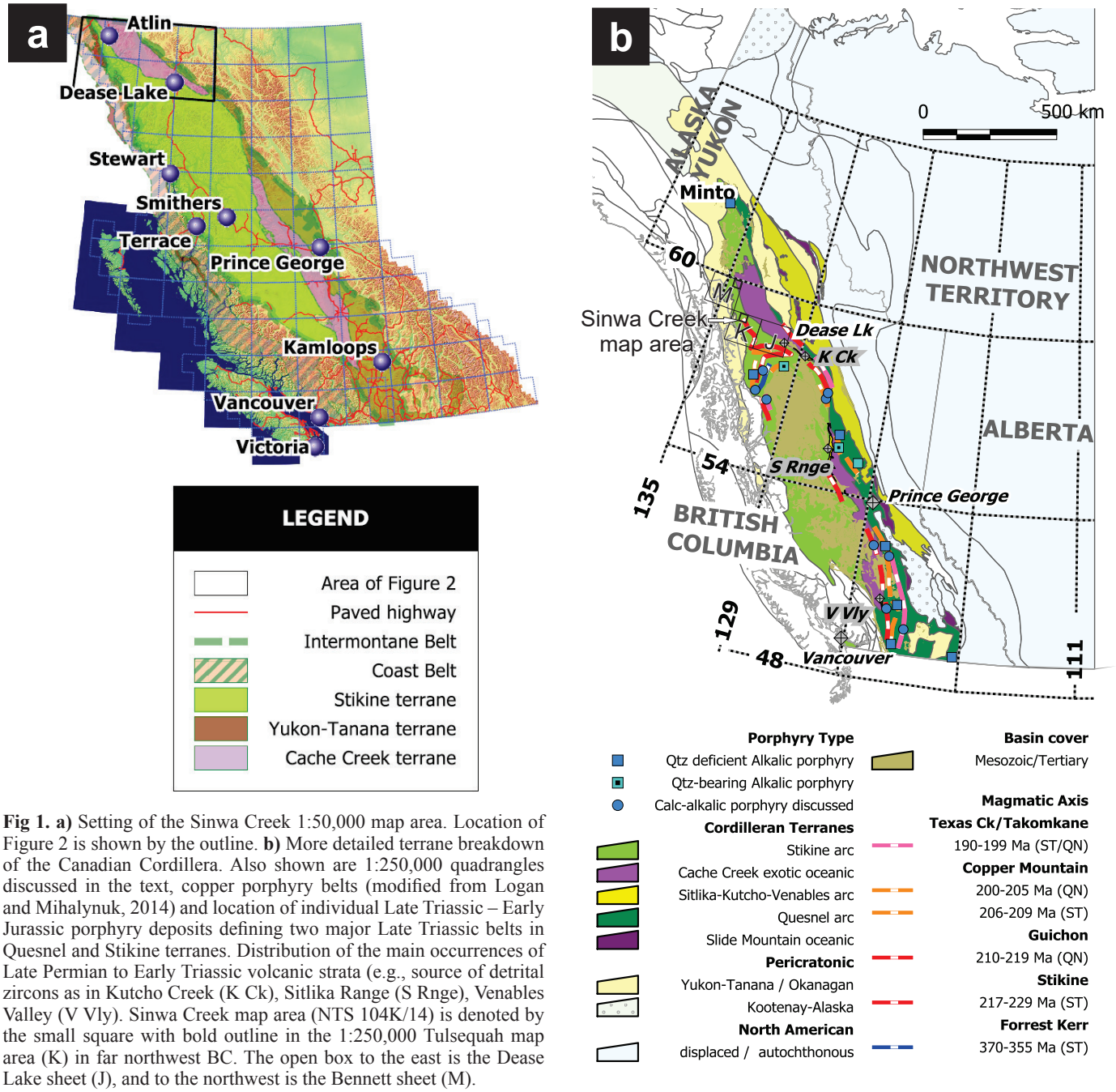

Fig 1. a) Setting of the Sinwa Creek 1:50,000 map area. Location of Figure 2 is shown by the outline. **b)** More detailed terrane breakdown of the Canadian Cordillera. Also shown are 1:250,000 quadrangles discussed in the text, copper porphyry belts (modified from Logan and Mihalynuk, 2014) and location of individual Late Triassic – Early Jurassic porphyry deposits defining two major Late Triassic belts in Quesnel and Stikine terranes. Distribution of the main occurrences of Late Permian to Early Triassic volcanic strata (e.g., source of detrital zircons as in Kutcho Creek (K Ck), Sitlika Range (S Rnge), Venables Valley (V Vly). Sinwa Creek map area (NTS 104K/14) is denoted by the small square with bold outline in the 1:250,000 Tulsequah map area (K) in far northwest BC. The open box to the east is the Dease Lake sheet (J), and to the northwest is the Bennett sheet (M).

we present findings from this mapping and geochronological analysis of two key units, tuff from the southeast corner of the map area (arc proximal) and strata immediately below an unconformity near the top of the Triassic section, as they pertain to the stratigraphic and structural evolution of the region.

2. Physiography and access

Sinwa Creek map area covers nearly 900 square kilometres at the transition between the coastal Boundary Ranges and the drier, more interior Taku Plateau. Southeast-flowing Sinwa Creek drains the center of the map area, merging with the Taku River about 6 km downstream of the Taku-Inklin River confluence (Fig. 3; also shown as Nakina-Inklin confluence on some maps). There are no roads or permanent settlements in the area, although buildings near the mouth of the Inklin River may be occupied during the fishing and hunting seasons. Shallow-draft boats can be used to access Taku and Inklin River valleys, but the most practical means of access is via helicopter with the nearest base 80 km to the north-northwest in Atlin. Juneau, Alaska is 90 km southwest.

3. Regional geology and previous work

Exploration of the area dates to 1887-1888 with the passage of prospectors up the Taku River en route to the Klondike

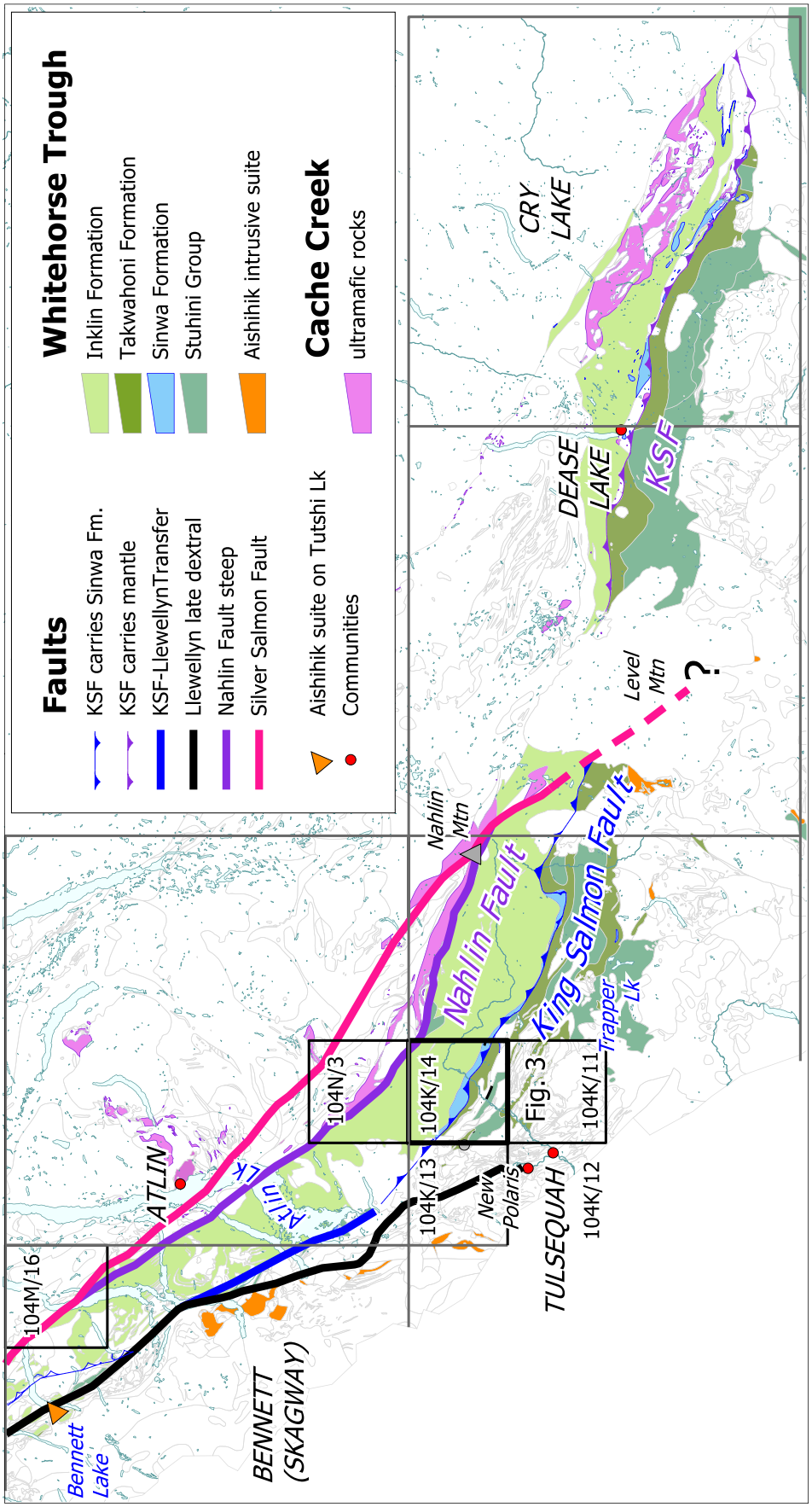

Fig. 2. Location of the Sinwa Creek map area in northwest BC with respect to crustal scale faults and key geological elements; Whitehorse trough strata of the Stikine terrane, and ultramafic rocks of the Cache Creek terrane (other units in these terranes are shown as grey outlines, no outlines for geology units comprising terranes to the east). Quadrangles discussed in text are shown. Large grid includes 1:250,000-scale quadrangles of Bennett, Atlin, Tulsequah, Dease Lake and Cry Lake map areas. Small quadrangles are 1:50,000 sheets: Sinwa Creek (104K/14, the focus of this paper); Turtle Lake (104M/16); and other sheets referred to in the text. King Salmon Fault is shown in two colours; where coloured blue it carries Sinwa Formation in its hangingwall, and where coloured purple (KSF) it also carries slivers of mantle rocks.

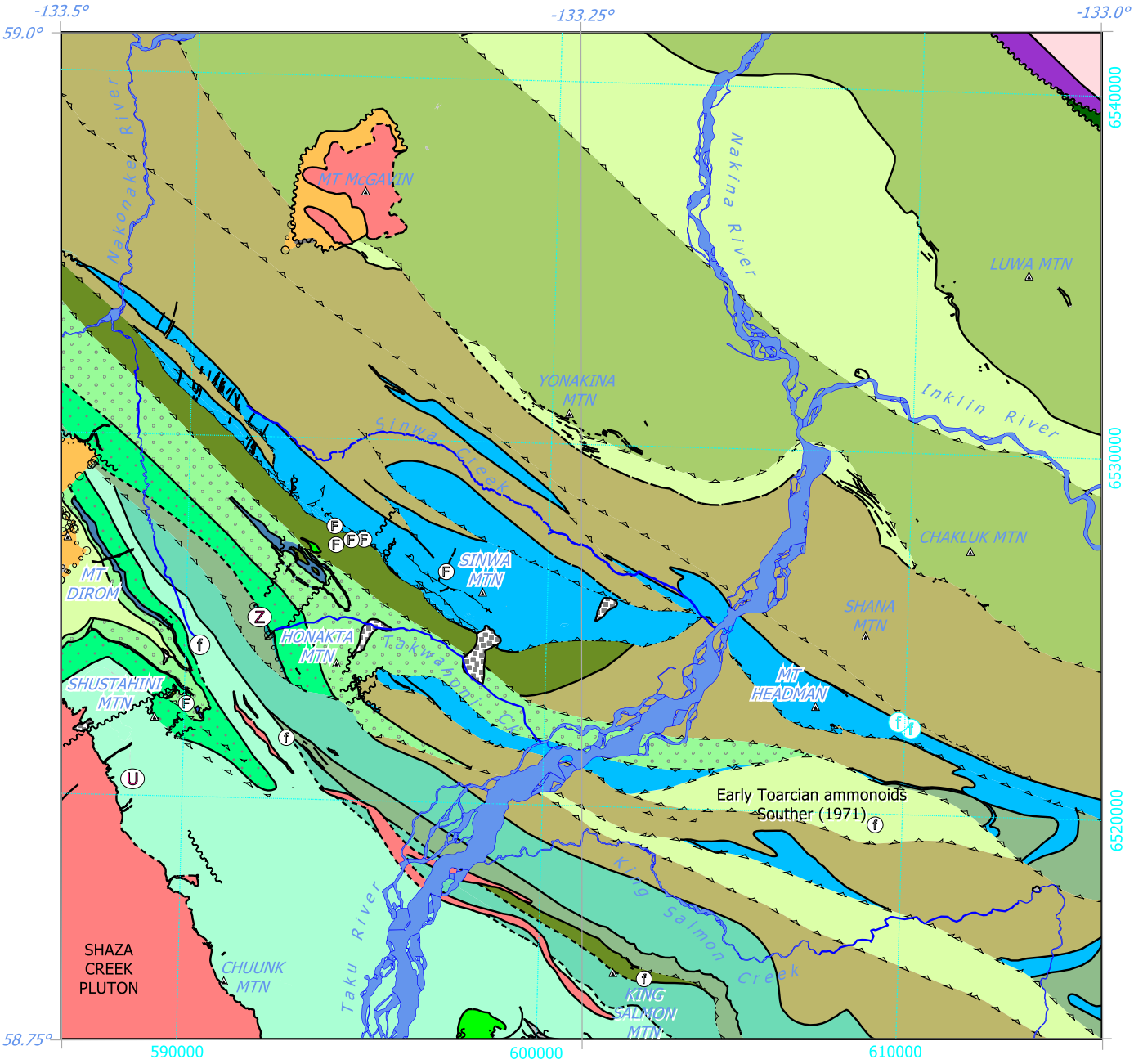

Fig. 3. Preliminary geology of the Sinwa Creek map area (104K/14).

goldfields. In 1923 and 1929, discovery of the Tulsequah Chief and Polaris Taku deposits led to establishment of a permanent mining town, complete with bowling alley, just 8 km from the southwest corner of the Sinwa Creek map area (Fig. 2). Systematic regional mapping of the region began with investigations by Kerr (1931a, b, 1948), followed by 1:250,000-scale mapping of the entire Tulsequah sheet in 1958 to 1960 by Souther (1971). Parts of the northeastern Sinwa Creek area were mapped by Monger (1975) who focused on Upper Paleozoic stratigraphy. Systematic 1:50,000-scale mapping in the area began in 1991 with reconnaissance surveys leading to coverage of the Tulsequah Glacier and Tulsequah River areas (104K/12 and 13; Mihalynuk et al., 1994 a, b), Stuhini Creek (104K/11, Mihalynuk et al., 1995 a, b) and Sloko River (104N/3, Mihalynuk et al., 2003a, b). These mapsheets surround the Sinwa Creek map area on all but its eastern side (Fig. 2). Unpublished mapping conducted as part of a Ph.D. thesis by English (2004) covered much of the alpine area northeast and within ~10 km of the prominent northwest-trending belt of Sinwa Formation limestone that bisects the Sinwa Creek map area.

Most of the Sinwa Creek map area is underlain by Late Triassic

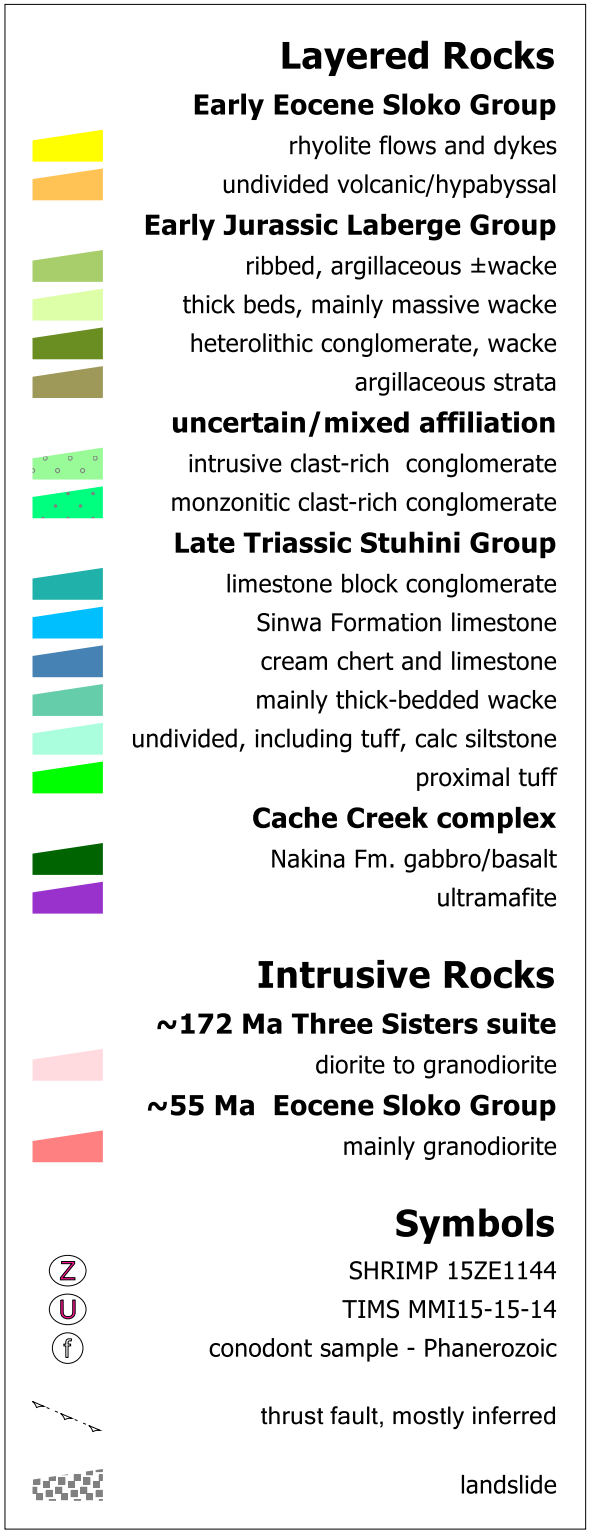

Fig. 3. Continued.

and Early Jurassic strata of the Whitehorse Trough (as defined by Wheeler, 1961; Figs. 2, 3). In the far southwest corner of the area is Eocene granodiorite of the Shaza Creek pluton (Souther, 1971; Mihalynuk et al., 1994), in the far northeast corner are oceanic crustal rocks and mantle rocks (Monger, 1975) of the Cache Creek terrane. In the northwest part of the map area, an outlier of Sloko Group volcanic rocks (Early Eocene) rests unconformably on deformed Jurassic strata and is cut by a presumably comagmatic quartz-monzonitic intrusion that underlies Mount McGavin (Fig. 3).

3.1. Terrane boundary constraints

Whitehorse trough marks the boundary between two major crustal terranes (Coney et al., 1980) of the Canadian Cordillera (Figs. 1, 2). To the northeast are oceanic crustal and mantle rocks together with exotic Paleozoic Tethyan marine strata of the Cache Creek terrane (Monger, 1977); to the southwest are the Paleozoic and Mesozoic arc strata of the Stikine terrane (Brown et al., 1991). However, the location of the terrane boundary within the Whitehorse Trough is debatable. Based on clast compositions in conglomeratic units that lie southwest of the King Salmon fault, affiliation with Stikinia has been argued (Johannson, 1993; Mihalynuk et al., 1995; Hart et al., 1995; Dickie and Hein, 1988; Johannson et al., 1997; Mihalynuk et al., 2004). These are rocks considered part of the Takwahoni Formation (Souther, 1971) which, together with more distal strata northeast of the fault (Inklin Formation) form the Laberge Group. Inklin Formation rocks have a less certain terrane affiliation. West of Atlin, the Inklin Formation is structurally interleaved with mid-ocean ridge-type pillow basalt and slivers of gabbro and serpentinized ultramafite (Mihalynuk et al., 1999).

Most workers have concluded that the Inklin Formation was deposited in the Stikine forearc (Dickie and Hein, 1995; Hart et al., 1995; Johannson et al., 1997; Bultman, 1979; Mihalynuk et al., 1999; Colpron et al., 2015), but evidence for arc construction spanning the Early Jurassic is lacking near 60°N, except for a magmatic pulse between 180-190 Ma represented in the Inklin Formation by layers of Nordenskiöld dacite (Cairnes, 1910; Nordenskiöld formation of Bostock and Lees, 1938; Colpron and Friedman, 2007; 186 - 188 Ma) or by their coeval and presumably comagmatic intrusive counterparts intruding basement rocks that flank the Whitehorse trough to the west, which include the Aishihik (Johnston and Erdmer, 1995; Johnston et al., 1996; see also, Fig. 2) and Long Lake (Woodsworth et al., 1992; Johnston et al., 1996) intrusive suites, and the Tagish intrusive suite in BC (Currie and Parrish, 1997). Detrital zircon age distribution peaks at 201 to 196 Ma have also been reported from the Laberge Group (Early Jurassic) in Yukon (Colpron et al., 2015), suggesting contributions from either nearby magmatic source rocks of this age, or ash from a more distal volcanic arc. We know of no discrete ash beds in the Laberge Group that have been isotopically dated as older than the Nordenskiöld dacite. Approximately coeval with these dacite tuffite layers are concentrations of feldspar porphyry clasts with a 'sooty' black matrix that Canil et al. (2006) found in some of the most inboard portions of the trough where ultra-high pressure (UHP) eclogite clasts (MacKenzie et al., 2005) of unknown provenance are also locally abundant in ~181 Ma Laberge Group strata (Zagorevski et al., 2015).

4. Stratigraphy

Late Triassic and Early Jurassic strata of the Whitehorse trough interfinger with and overlie volcanic rocks of the Stuhini arc (Late Triassic), which underlie parts of southwestern Sinwa Creek map area and Stuhini Creek map area to the south. Although folds and thrust faults complicate relations, strata generally become less proximal, dip regionally, and young to the northeast, away from the apparent arc axis. The stratigraphic and facies progression from mainly Late Carnian volcanic Stuhini Group (Souther, 1971) is: coeval flanking and overlying volcano-sedimentary rocks, capped by the Upper Norian Sinwa Formation, unconformably (?) overlain by Pliensbachian to Toarcian conglomeratic Takwahoni Formation (southwest of the King Salmon fault), and wacke and argillite of the Sinemurian to Pliensbachian Inklin Formation (northeast of the King Salmon fault). Conglomeratic units including those dominated by monzonitic volcanic and intrusive clasts overlap units originally mapped by Souther (1971) as Stuhini Group (including volcanic rocks and his 'King Salmon Formation' clastic strata). These conglomeratic units apparently overlie a Late Triassic unconformity, and on that basis, are probably Early Jurassic in age, but conclusive age data are lacking. Until such data are available, we refer to the conglomerate units as having 'uncertain/mixed affiliation' (Fig. 3). Youngest strata of the Laberge Group, Middle Jurassic (Aalenian to Bajocian) chert pebble conglomerate derived from Cache Creek terrane (Souther, 1971; Mihalynuk et al., 2004), are known to the south, but have yet to be identified in the Sinwa Creek area. Early Eocene volcanic strata of the Sloko Group unconformably overly the Whitehorse trough as scattered outliers at high elevations. These volcanic strata have been described where they extensively crop out in adjacent map areas (Mihalynuk et al., 1994; Mihalynuk et al., 1995); therefore, descriptions are not repeated here.

4.1. Stuhini Group

West-northwest-trending limestone beds of the Sinwa Formation (Late Norian, Souther, 1971) form a conspicuous unit that caps the Stuhini Group and divides the Sinwa Creek map area diagonally in two. Structurally below the Sinwa Formation are distinctive conglomeratic, volcanogenic and minor, but prominent, limestone strata that may correlate regionally. Units mapped in the Sinwa Creek area are described here, from southwest to northeast, mainly from oldest to youngest, except for probable thrust duplication (see below, King Salmon fault).

4.1.1. Tuff at Chuunk Mtn.

Stuhini Group in the Chuunk Mountain area (Fig. 3) consists of light green to maroon interlayered andesitic tuff breccia to crystal tuff. Tuff breccia horizons are polylithic and include massive, vesicular, feldspar and/or hornblende porphyritic andesite blocks that range from angular to amoeboid. Within the same beds, the colour of the clasts varies from green to maroon. Finer tuff layers are locally pervasively hematized and contain angular, white feldspar crystal-rich laminae that exhibit both normal and reverse grading. Laminae are locally truncated by volcanic blocks, and also exhibit local sags and/or draping. Massive tuff beds >4 m thick, amoeboid blocks, apparent volcanic bombs, and inversely graded layers suggest an explosive, vent-proximal volcanic environment. Hematized blocks and beds are common, consistent with oxidizing conditions in subareal or shallow marine settings. A sample of massive lapilli tuff collected for U-Pb isotopic analysis (15ZE1144) returned an age of 217.49 +0.31/-0.44 Ma (see below, Geochronology).

4.1.2. Well-bedded calcareous siltstone

Orange-weathering, well-bedded calcareous siltstones occur at several stratigraphic levels and are generally included in Figure 3 as part of the 'undivided' Stuhini Group. In the region near Shustahini and Honakta mountains, brown to orange-weathering, well-bedded calcareous siltstone is the predominant unit. Planar interbeds of massive wacke and lenses of conglomerate containing boulders of coarse augite porphyry and beds of impure, orange-weathering limestone, all from ~1 m to ~10m thick, are locally important constituents. Siltstone beds are typically 1-10cm thick with parallel laminae; although they can display good cross stratification. Marley beds are common. Where bedding planes part cleanly, well-preserved ammonites and paper clams (*Halobia*?) can be found with a little searching. Where this unit occurs structurally above the monzonitic clast-rich conglomerate it contains distinctive layers of gastropod packstone. At their thickest, these layers form ~20 cm beds packed with gastropods 2-3 cm across (Fig. 4).

Owing to their distinctive and easily recognized appearance, these beds, and the carbonate-rich siliciclastic interval in which they occur, could make a useful regional marker. However, the two localities where this lithology has been observed are both structurally disrupted and their stratigraphic position is uncertain. Thus, on Figure 3 we include them in the "undivided,

Fig. 4. Distinctive, orange-weathering gastropod packstone with matrix composed of volcanic sand grains in micrite.

including tuff, calc siltstone" unit, designating the fossil rich layers with an "F" (at Shustahini Mountain, where the unit is too restricted to show at the map scale).

Based on previous fossils reported from this part of the map area (Souther, 1971) and unconfirmed field identification, we suspect that this unit is Late Triassic. However, changes in younging directions within the mainly homoclinal succession at Honakta Mountain (Fig. 3) suggests that cryptic isoclinal folds repeat at least parts of the unit.

Generally fine grain size suggests deposition as some distance from source terrains, and possibly in relatively deep water. However, based on modern analogues, gastropods are photic zone grazers and such abundant fossil remains points to a shallow-water environment. Lack of broken shells suggests a quiet, possibly lagoonal or estuarine setting with siliciclastic input. High carbonate content may represent background carbonate productivity. Relatively pure carbonate accumulated when siliciclastic input waned, as indicated by gradations on metre scales from siltstone to limestone.

4.1.3. Black, friable argillite

Dark brown to black, locally petroliferous argillite underlies the main Sinwa Formation carbonate layer west of Sinwa Mountain. Thin bedding tends to break into centimetre-scale pieces creating friable, recessive outcrops. Black argillite probably grades into orange- and black-weathering, finely bedded argillite and siltstone structurally down section. However, abundant low- and high-angle faults preclude establishing stratigraphic continuity. About 200m structurally down section are coarse wacke and intrusive clast-rich conglomerate layers (Fig. 5). No macrofossils were recovered from the argillite-siltstone section.

The black argillite unit may have been a detachment surface during thrust repetition of the apparently overlying Sinwa Formation. On the southeast flank of Sinwa Mountain, the main mass of carbonate rocks can be seen in imagery to grade into underlying dark siliciclastic strata, probably equivalents of this unit. Thrust slivers of the unit are too thin to portray on Fig. 3.

4.1.4. Sinwa Formation

Sinwa Formation limestone is beautifully exposed on the glacially sculpted ridges (Fig. 6) underlying Sinwa Mountain, extending northwest to the Nakonake valley, and more than 50 km southeast to the headwaters of the Inklin River. Typically light grey-weathering and massive, well-bedded sections occur near the base and middle of the formation (Fig. 6). Some distinctive horizons, such as a petroliferous, colonial coral packstone (Fig. 7a), can be traced for kilometres, commonly terminating at faults. We estimate that the Sinwa Formation is at least 2000 m thick, but structural disruption leading to thickening and stratigraphic omission can be cryptic, and detailed sections were not measured. Extensive karsting has led to modern collapse features, sinkholes, and influent or disappearing streams.

Massive limestones are predominant and locally contain

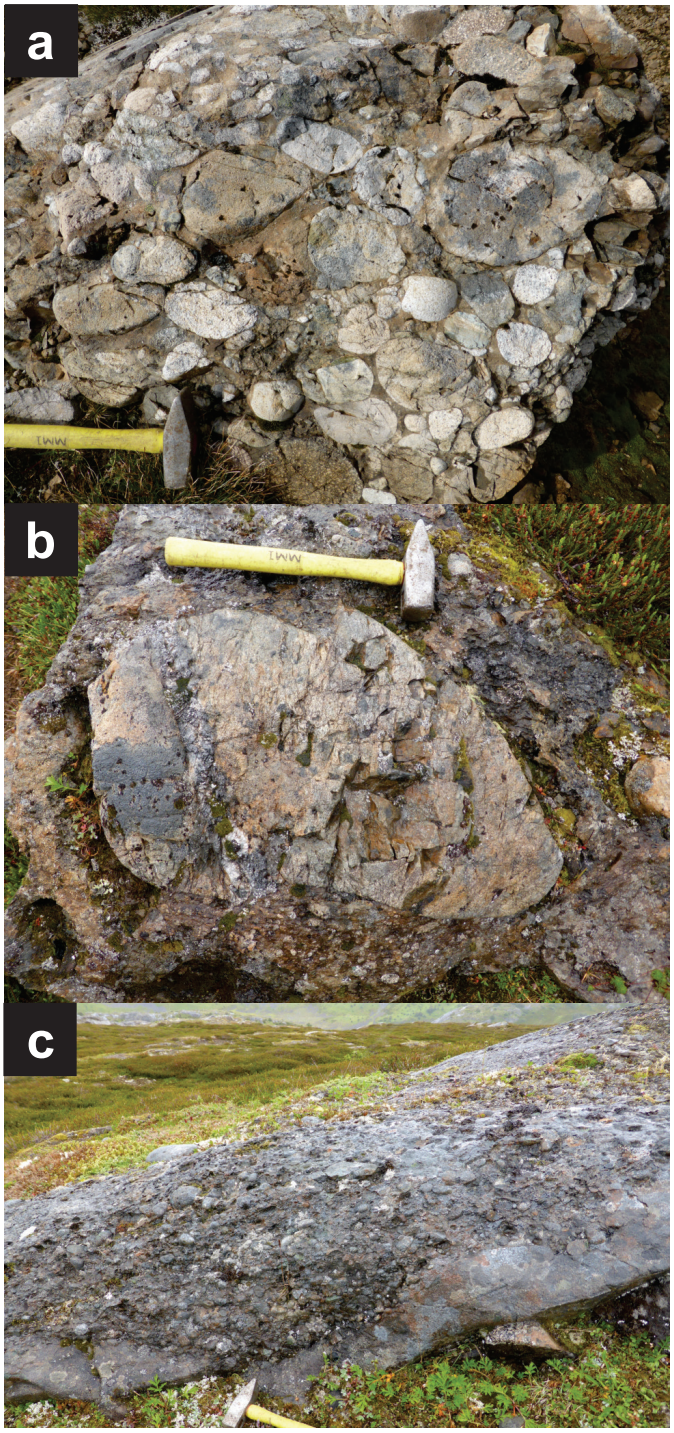

Fig. 5. Intrusive clast-rich conglomerate. **a)** Near Takwahoni Creek. **b)** Near Sinwa Mountain. **c)** Also near Sinwa Mountain, a conglomerate bed with erosional base cutting underlying coarse wacke beds.

nodular chert in crudely layered zones tens of metres thick. These massive limestone units form the top of at least two major depositional cycles and are locally coralline (Fig. 7b). In the lower cycle, dark fine-grained siliciclastic strata grade to limestones, with the number and thickness of limestone beds increasing upsection. The cycle is capped by sparsely bioclastic limestone beds, locally with colonial corals, metres to about ten

Fig. 6. View to the east, oblique to the strike, with light grey-weathering Sinwa Formation limestone in the near horizon. White-weathering mountain face in the centre, far horizon is Mt. Sinawa Eddy, mainly Permian Tethyan limestone of the Cache Creek terrane. Cream-weathering chert-limestone unit at the left center cores a southwest-verging fold outlined by dark grey-weathering intrusive clast-rich conglomerate (chert-limestone enclosed by cyan dashed line). Light weathering rocks in the foreground are monzonitic clast-rich conglomerate.

metres thick. At the base of the second cycle, limestones are abruptly overlain by siliciclastic rocks that weather dark grey, brown and locally maroon (Fig. 8). Breccia zones are common. Some are localized along faults, but others form lobes that may be hundreds of metres across. Breccia lobes truncate adjacent strata and are draped by overlying limestone beds (Fig. 8). Rare laminated, cream coloured cherty beds less than 1m thick are similar to those that predominate a cream chert and limestone unit structurally below (southwest of) the main belt of Sinwa Formation.

Few fossil collections from the Sinwa Formation at its type locality have been sufficiently well studied to yield ages to the stage level. Souther (1971) noted only two such collections, neither from Mount Sinwa (from near King Salmon Lake, southeast of the Sinwa Creek map area), both 'Upper Norian'. Late Norian to Rhaetian (*Epigondolella englandi*) conodonts have also been recovered from a discontinuous belt of limestone bodies extending from the Yukon border to southern Atlin Lake (Mihalynuk, et al., 1999). This belt continues into Yukon where reef mound buildups are well exposed, such as at the famously fossiliferous Lime Peak reef, north of Whitehorse (Yarnell et al., 1998; Reid and Tempelman, 1987).

4.1.5. Cream chert and limestone

Distinctive cream-colouration of a chert and limestone unit together with extensive talus fans permit them to be easily distinguished at a distance from limestones of the Sinwa Formation (Figs. 6, 9a). Thickness varies from ~110 to 180 m, although structural thickening and thinning are likely. The chert and limestone form discrete interbeds a decimetre or more thick (Fig. 9b). Resistant laminae are common on chalky weathered surfaces of the chert beds.

A stratigraphic contact between the cream chert-limestone unit and an underlying intrusive clast-rich conglomerate unit (see below) cannot be unequivocally demonstrated, but if depositional, an abrupt change in environment is implied. The

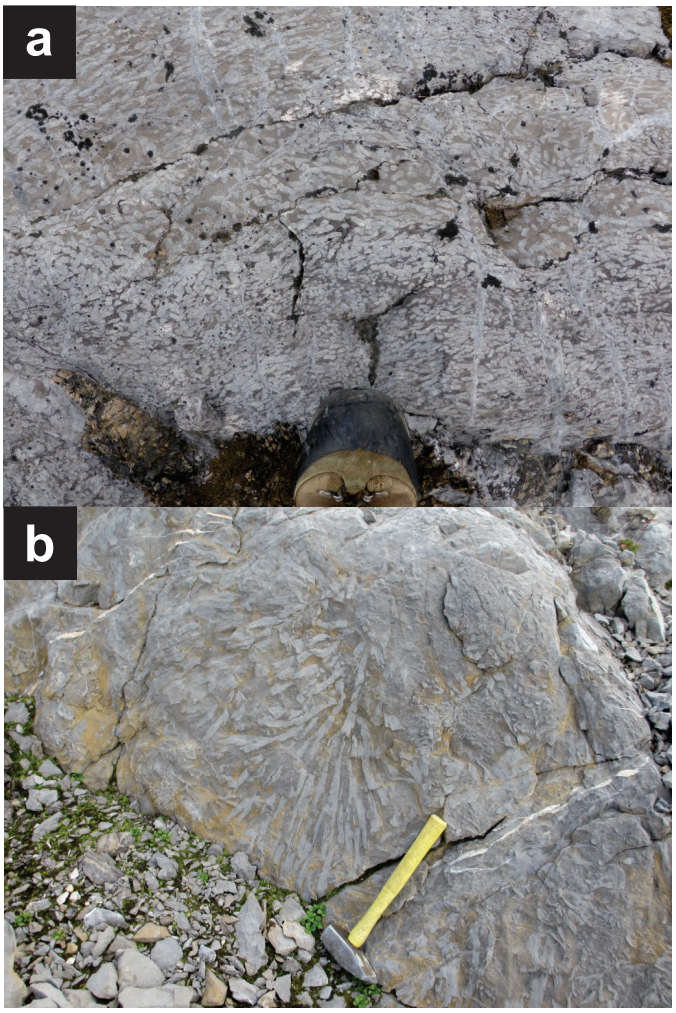

Fig. 7. a) Colonial coral packstone, probably *phaceloid Retiophyllia* sp., based on similarity with samples identified by G. Stanley (written communication) from a petroliferous, well-bedded Sinwa Formation sample. **b)** Branching coral.

age of the unit is unknown, but based on similar sparse beds in the Sinwa Formation, a Norian age is inferred.

4.1.6. Limestone block conglomerate

On the northwest flank of Honakta Mountain, a distinctive limestone block conglomerate (Figs. 10a, b) marks the unconformable contact between a well-bedded predominantly siltstone section and overlying volcanic sandstone and conglomerate. Light grey-weathering bioclastic limestone blocks comprise 70-90% of the clasts and can be more than a metre across (Fig. 10a), far larger than any other clast type. However, in the cirque face to the north, light grey blocks ~5m in long dimension can be seen from afar (Fig. 10c). Coral, crinoid, bivalve and fish bone fossils are well preserved in many of the blocks. Identification of these fossils is pending.

Other common clasts include porphyritic intrusive clasts, with mainly feldspar, lesser hornblende ±pyroxene, and quartz grains. Attaining boulder size, they are typically well rounded, in contrast to many of the limestone clasts, which can be highly angular or even have delicate appendages (Fig. 10b).

Based on paper clams in underlying strata and *Halobia* identified on the west side of Honakta Creek, as well as Early Jurassic fossils in strata correlated with the overlying conglomerates of Takwahoni Creek (Souther, 1971), a Late Triassic, probably Late Norian age is suggested. A medium-grained sandstone bed beneath the conglomerate was collected for detrital zircon age determination to test this age assignment, but unexpectedly returned a nearly unimodal population of Middle Triassic zircons with a peak at ~242 Ma (see below, Geochronology) which requires special circumstances for deposition in a Late Triassic forearc environment (see below, Discussion).

Some limestone blocks show evidence of post deposition compaction and may have been deposited in a semi-lithified state (Fig. 10b). Semi-lithified limestone blocks metres across are most likely olistostromal deposits. Admixture of rounded boulders of monzonite point to the combination of sediments from intra and extra-basinal sources, as may have occurred during collision and uplift of the carbonate bank. Rounding of boulders is not necessarily an indication of long distance alluvial transport because spheroidal weathering of jointed rocks in tropical environments produces rounded blocks at the outcrop source (e.g., Hall and Smyth, 2008).

4.2. Uncertain/mixed affiliation

Conglomerate units here grouped as 'uncertain/mixed affiliation' have been mapped by Souther (1971) as Takwahoni Formation (Early Jurassic) and as Stuhini Group (Late Triassic).

4.2.1. Monzonitic clast-rich conglomerate

Conglomerate containing predominantly monzonitic clasts is well exposed at the headwaters of Takwahoni Creek where a structural thickness of ~1.2 km is exposed. Although low-angle faults cut the section, the amount of structural thickening is unknown. Conglomerate beds are tabular to lensoid. The unit can be easily identified based on characteristic white to pale pink-weathering, porphyritic clasts (locally maroon to green), which weather lighter than the matrix. Clasts are commonly acicular hornblende and tabular feldspar porphyry (Fig. 11a). Fine-grained to aphanitic green and maroon clasts may comprise up to ~2% of typical outcrops. Clasts are pebble and cobble sized, ranging to boulder sized (Fig. 11b). Interbeds of sandstone and tuffite display both sharp and gradational contacts with conglomerate. Within dense conglomerate bed interiors, the tuffaceous sandy matrix is weakly- to non-calcareous, but where the unit becomes orange-tinged, it is commonly calcareous. Viewed from a distance, layers containing megaclasts up to ~7 m across, can be identified (Fig. 11c). Near contacts with the underlying limestone block conglomerate (see above) this unit includes ~10 m sections of green volcanic sandstone with white alteration spots.

To the east, in the headwaters of Sinwa Creek, beds with lapilli and ash-sized monzonitic fragments are interpreted as distal equivalents of the conglomerate. Green argillaceous layers

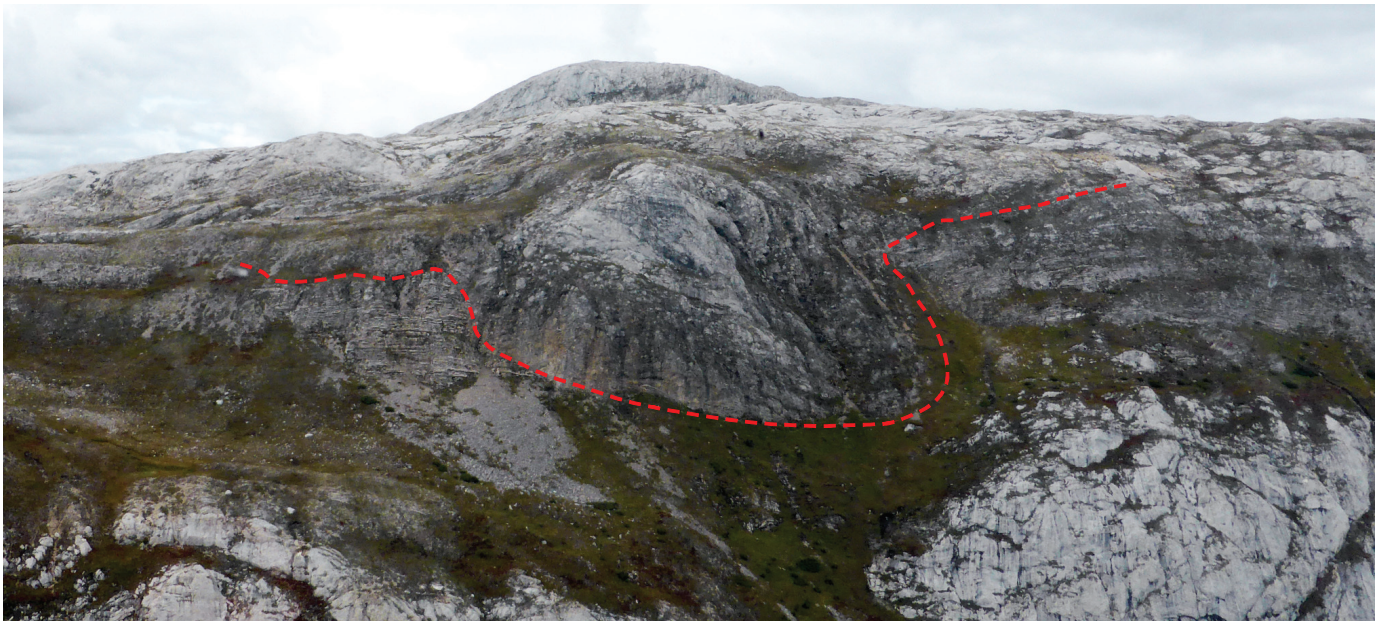

Fig. 8. View to the northeast of a megabreccia lobe that truncates well-bedded limestone of the Sinwa Formation. Dashed red line follows the approximate base of the unit and beginning of successive depositional cycle with massive limestone near its base.

Fig. 9. a) View along strike to the northwest of cream-weathering chert and lesser carbonate at Mt. Dirom dip steeply to the west and are unconformably overlain by dark brown to maroon flow and interflow breccia of the Sloko Group (Eocene; Nakonake formation (above dotted lines) cf. Mihalynuk et al., 1994). In addition to the distinctive cream colour, this unit produces talus slopes (blue arrows), unlike the relatively pure carbonate rocks of the Sinwa Formation, which tend to erode by dissolution. Massive thick units enclosing the chert are intrusive boulder conglomerate layers, stained deep maroon by iron oxides below the unconformity. Recessive strata in the col at the centre of the photo are thinly bedded argillaceous strata of uncertain, but presumed Early Jurassic age. Thick conglomerate beds east of the chert and lesser carbonate unit appear truncated by the unit, perhaps by an east-directed back thrust. **b)** Close-up of laminated, cream chert beds and a light grey interbed of fine-grained, recrystallized limestone.

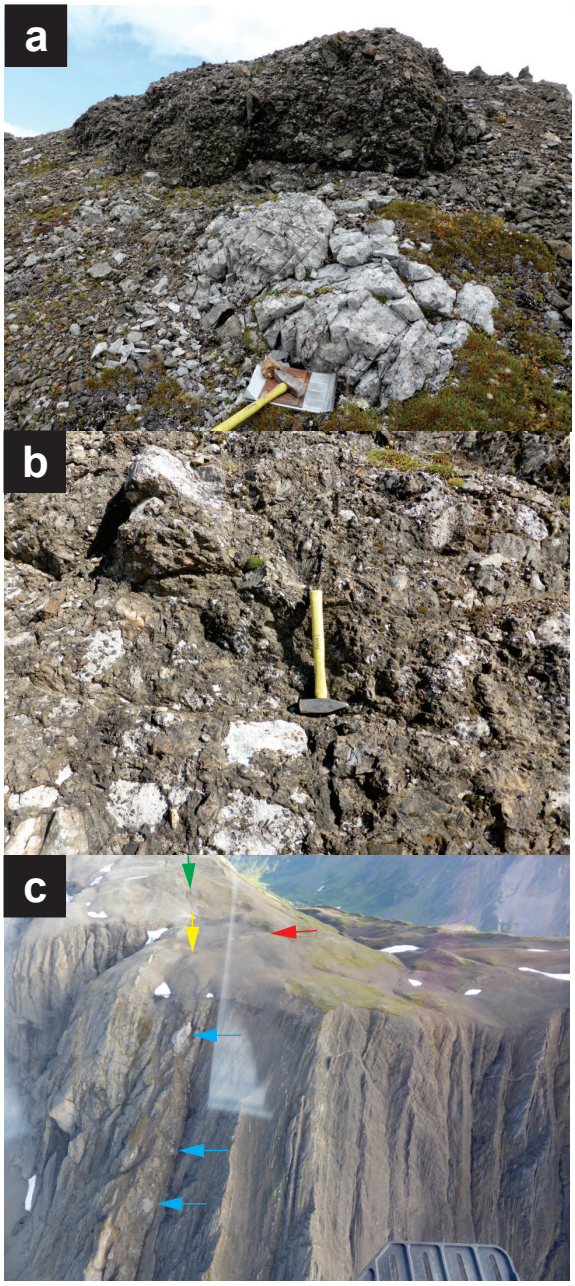

Fig. 10. a) Limestone boulder conglomerate that contains blocks more than a metre across (e.g., light grey limestone clast that the clipboard is resting against). Rubble of slope is composed of boulders weathered out of the conglomerate. **b)** Many limestone clasts have irregular outlines (e.g., below left of hammer) suggesting deposition in a semi-lithified state. In contrast, most intrusive boulders are well rounded (e.g., see top of outcrop in a). **c)** Southward overview through helicopter window (note reflections) of the unconformity between calcareous Late Triassic *Halobia*-bearing argillite (brown on right) and siltstone and monzonite clast-rich conglomerate and volcanic sandstone (grey, to left). Blue arrows point to very large limestone blocks in the conglomeratic unit. Green arrow shows location of coarse conglomerate as it strikes southwest across the plateau. Yellow arrow is approximate site of sample collected for detrital zircon age determination (MMI15-15-14). Red arrow denotes a dike that cuts section (continues to behind yellow arrowhead), part of an extensive dike set that can also be seen farther west on the plateau and cutting well-bedded Late Triassic strata in the cliff section.

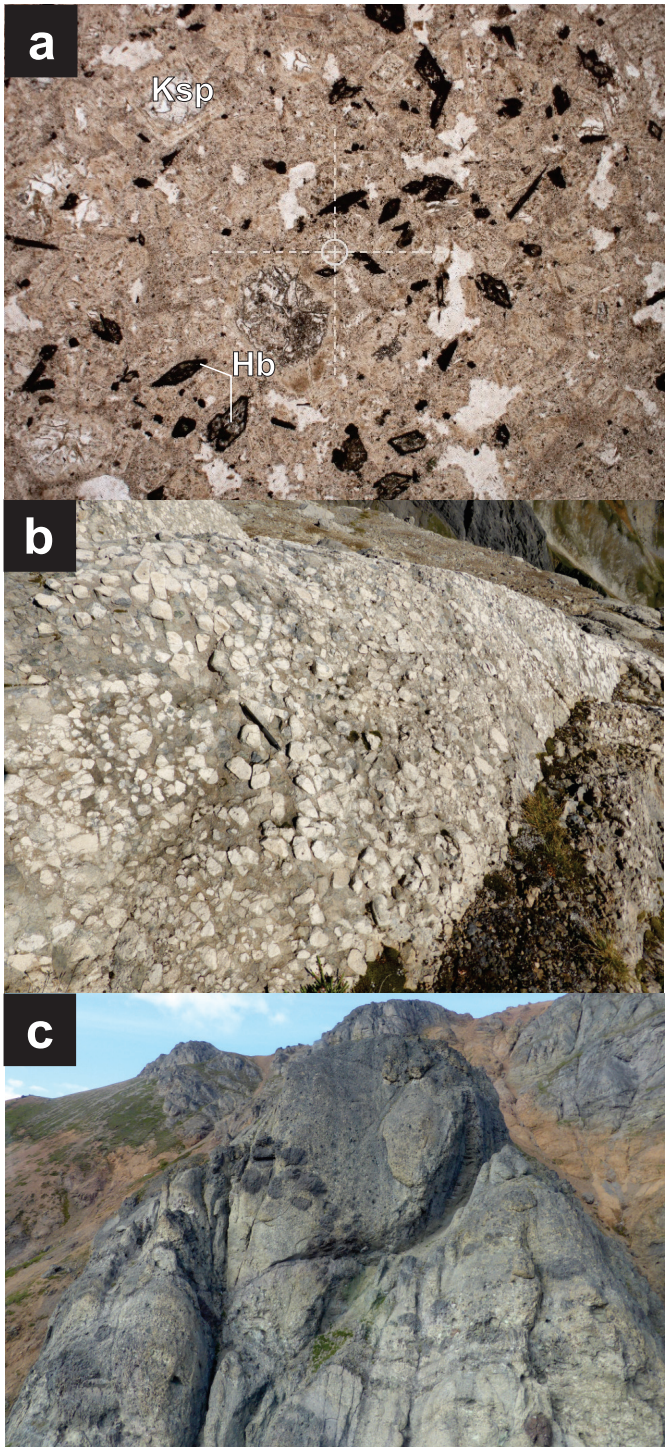

Fig. 11. a) Thin section of monzonite clast conglomerate. Hb=hornblende, Ksp=K-feldspar, in plane-polarized light; width of photomicrograph represents ~4 mm. The circle at the cross hairs has a radius of 100 microns. **b)** Outcrop of monzonite clast-rich conglomerate showing typical white to light tan pebbles, cobbles and boulders. **c)** View eastward of megaclast conglomerate in the monzonite clast conglomerate. Height of the near cliff face is about 30 m (aerial reconnaissance not confirmed by on-the-ground observations). Megaclasts in the cliff face are both darker and lighter (largest clast, ~7 m, near peak) than the enclosing strata. A megaclast-bearing unit outside the field of view to the right (southwest) contains mainly limestone blocks (not the same layer as shown in Figure 10).

millimetres thick display possible desiccation cracks infilled by volcanic sandstone (Fig. 12). The coarse conglomerates were derived from a restricted, relatively homogenous igneous source area and probably deposited in a fan-type submarine to locally subaerial setting.

Fig. 12. Carbonate-altered tuffaceous sandstone with mud interlayer that appears to have been cracked (view of top of muddy layer), possibly due to desiccation during subaerial exposure.

4.2.2. Intrusive clast-rich conglomerate

Thick sections of intrusive clast-rich conglomerate crop out extensively west of the Sinwa Formation. Internally, bedded layers can be more than 260m thick (e.g., the northeast flank of Mount Dirom). Clasts range from coarse K-feldspar-rich granitoids to medium-grained plagioclase, and quartz-eye and plagioclase quartz-eye porphyries (Figs. 5a, b). Hornblende can comprise up to ~15% of the porphyritic clasts and is generally intensely chloritized. The unit locally contains volcanic sandstone beds and thin maroon beds with variegated lapilli- and ash-sized fragments in a fine tuffite matrix. Some tabular beds display erosional, channeled bases (Fig. 5c). At Mt. Dirom and along strike at Shustahini Mountain, conglomerates are in contact with a cream-coloured limestone-chert unit, or nearly so (Fig. 9a). Unfortunately, a lack of clear sedimentary younging indicators and concentration of strain along the contact, renders the stratigraphic relationship ambiguous. A complete lack of cream chert clasts in the adjacent boulder conglomerate unit where it has been mapped suggests that either the chert-limestone unit was deposited atop the conglomerate, or the contact is a bedding-parallel fault with considerable offset. Abrupt lateral truncation of conglomerate layers on the east flank of Mt. Dirom points to an east-directed thrust fault (Fig. 9a).

4.2.3. Mainly thick-bedded wacke

Dark olive-brown wacke beds up to ~10m thick can form featureless cliff bands. Volcanic-lithic and feldspar grains are the most common constituents. In some localities fine-grained feldspar porphyry clasts with indistinct clast outlines comprise a significant proportion of the beds. Angularity of these volcanic clasts suggests a proximal source with minor reworking; some accumulations of volcanic debris may be subaqueous tuff. Sets of massive wacke beds form resistant ribs that extend northward into the Nakonake River valley and are readily visible on satellite images.

This unit was mainly mapped as Stuhini Group by Souther (1971), but is lithologically similar to wacke of the Laberge Group. Nevertheless, until fossil or isotopic data confirm an Early Jurassic age, we retain this unit as part of the Stuhini Group.

4.3. Laberge Group

Structurally and stratigraphically above the Sinwa Formation, most sections are composed of varying proportions of massive wacke, argillite, siltstone and minor conglomerate, all with variable matrix carbonate contents, which we include with the Inklin Formation of the Laberge Group (as did Souther, 1971). The Inklin Formation can be divided into two major units: predominantly massive volcanic wacke which is thick-bedded and blocky; and argillaceous strata ± wacke, which is medium to thin-bedded and weathers into strongly ribbed outcrops. Distinctive, eclogite-clast-bearing beds that occur in the massive wacke unit along strike to the northwest (English et al., 2005; Canil et al., 2006; MacKenzie et al., 2005) are apparently lacking in the Sinwa Creek area.

Less abundant units include, argillite-siltstone couplets, and coarse conglomerates, and these can locally be the principal rock type over tens of metres of section. Limestone is uncommon, occurring as thin interbeds in argillaceous strata, and rarely, as massive beds tens of metres thick, as at Mount Luwa (Fig. 3). Along strike to the northwest, Inklin Formation units have been thoroughly described by previous workers (Dickie et al., 1992; Mihalynuk et al., 1999; Hart, 1997; Johannson et al., 1997) and only the main units are summarized briefly below.

4.3.1. Massive to well-bedded wacke

Feldspathic wacke forms massive beds decimetres to metres thick, with rare beds 10 or more metres thick. Beds tend to be planar, but can also be lensoid. Scoured bases are locally well developed, and lower parts of the beds may contain abundant wacke intraclasts. Individual beds display graded bedding and rare ripple or trough cross stratification near their tops. Granules and pebbles of finely-porphyritic volcanic and intrusive derivation commonly form diffuse layers, typically less than a few pebbles thick, within otherwise massive wacke beds. Detrital quartz can locally comprise 10% of beds, typically together with orthoclase and detrital biotite, indicating a granitoid source terrain. Propylitic alteration of some igneous clasts indicate derivation from an altered source.

Interbeds of coarse feldspathic sandstone, siltstone, and shale can range from centimetres to many metres thick (Fig. 13). Wacke is also interbedded with, and less commonly grades into, cobble conglomerate across bedding widths of decimeters to metres. Argillaceous wacke-supported conglomerate beds

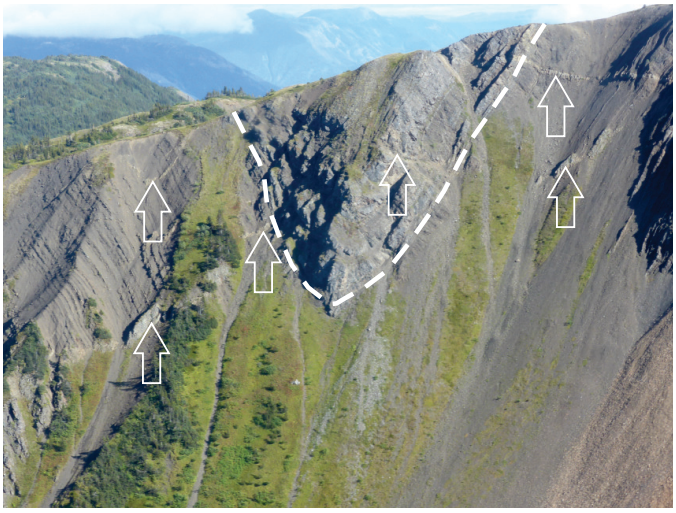

Fig. 13. Thick-bedded wacke in core of syncline (white dashed line) enveloped by dark brown, argillaceous siltstone. Cutting the section are two light-weathering sets of dikes (white arrows, probably Eocene).

Fig. 15. Black and tan rhythmite in the Whitehorse trough. This is a characteristic lithology of the Richthofen formation in the Yukon, which has been mapped southward into BC to ~59.5°N (Johnston et al., 1999).

commonly contain well-rounded limestone, granite and rare chert clasts, suggesting recycling of the Triassic sedimentary rocks.

4.3.2. Argillite – siltstone

Well-bedded siltstone sections commonly display beautiful cross stratification, both trough cross stratification and climbing ripples (Fig. 14). Beds are generally 0.5-5 cm thick and tend to be laminated. They weather orange and black and are typically strongly calcareous. In some sections, abundant 2-3 mm wide wormy trace fossils cover bedding surfaces. Sparse paleoflow directions, as determined from trough axes, tend to be from the northwest or west.

Sections of tan and black rhythmites (Fig. 15) have been mapped northwest, west and south of Atlin (Mihalynuk et al., 1999; Johannson et al., 1997; English et al., 2003, 2005; Wight et al., 2004) and are known in Yukon as one of the diagnostic rock types in the Richthofen formation (Tempelman-Kluit, 1984; Lowey, 2003, 2004). Siltstone-argillite couplets form graded layers 1-5 cm thick; some layers have bases of fine- to medium-grained sandstone. Vermicular trace fossils are locally well preserved in the argillite. Cleavage is commonly well-developed in this lithology, leaving only fragmentary bedding surfaces preserved. These rhythmites were interpreted by Lowey (2004) as distal turbidites deposited in a submarine fan complex, representing outer-fan levee and interchannel/interlobe sedimentation.

Fig. 14. Trough cross stratification in calcareous siltstone of the Laberge Group indicating paleoflow to the east or southeast.

5. Sloko (?) dikes

Porphyritic dark greenish-grey, orange to green-weathering, subvertical dikes (2.5-6 m thick) are interpreted to be subvolcanic equivalents of the regionally extensive Sloko Group. The dikes are most obvious where they cut the Sinwa Formation (Fig. 3) where they have sharp, chilled contacts. They are medium grained (lesser coarse grained) and contain tabular and glomeroporphyritic feldspar (30-40%) and ~2-5% equant chlorite clots, probably derived from fine-medium grained pyroxene. Dike interiors commonly weather recessively (Fig. 16a). Silicification of limestone adjacent to the dikes can be intense, and some silicified zones contain bladed calcite characteristic of epithermal alteration (Fig. 16b). Preliminary geochemical analyses do not indicate precious or base metal enrichment. Further analyses are pending.

Dike orientations are predominantly north-northeast, and they probably fed a volcanic carapace that has been eroded away, except for a ~15 km^2 relict underlying the flanks of Mount McGavin. Sloko Group volcanic rocks are more extensive in map areas to the west and south where they have been described in detail (see Mihalynuk et al., 1994; Mihalynuk et al., 1995).

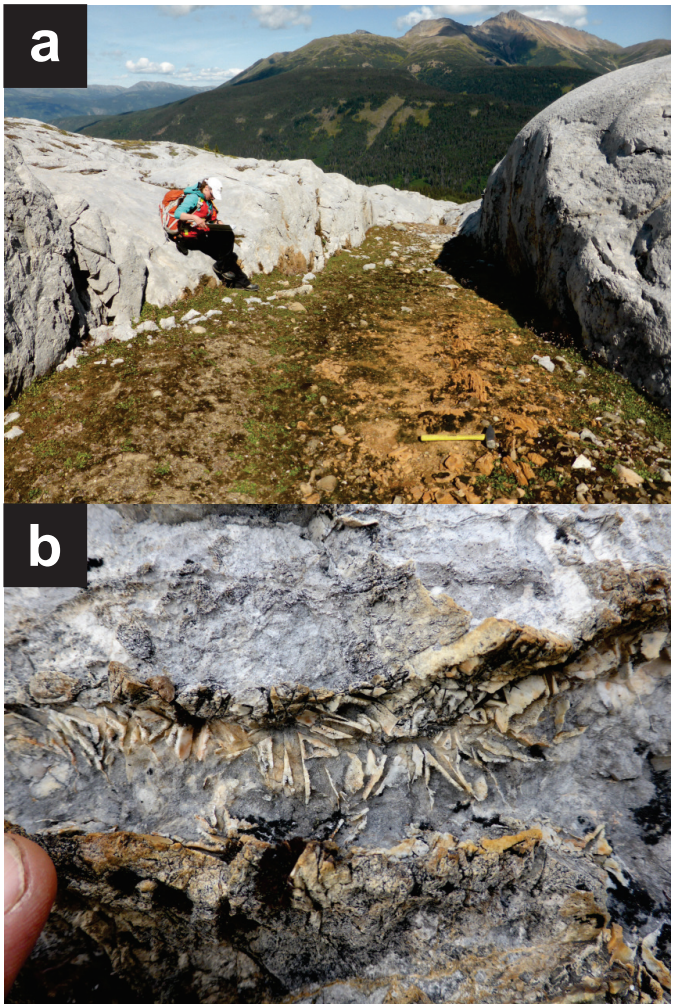

Fig. 16. a) North-trending, sub-vertical, orange-weathering, recessive, mafic dike (presumably Early Eocene) cuts Sinwa Formation (Fig. 3). It is part of a regional swarm interpreted to have fed Sloko volcanic strata, such as the those capping Mt. McGavin on the horizon. **b)** Joints in adjacent wallrocks above where the dykes solidified display evidence of hydrothermal activity. Bladed calcite in a matrix of finer-grained calcite may indicate boiling, which can cause gold and other metals to precipitate. Samples collected from this bladed calcite carried neither elevated Au nor other metal values.

6. Geochronology

Between the Taku River area and Yukon, strata in the hangingwall of the King Salmon fault (Hart et al., 1995; Johannson et al., 1997; Mihalynuk et al., 1999; Colpron et al., 2015) are well-dated. In contrast, age control in the footwall are relatively sparse (Souther, 1971; Mihalynuk et al., 1995). To address this imbalance, we collected samples with fossil invertebrates and material for microfossil determination (identifications are pending). We also collected two samples for U-Pb geochronology, one from tuffaceous strata north of Chuunk Mountain (Fig. 3; see Section 4.1.1.), and one from a coarse, quartz-rich sandstone unconformably below the limestone block conglomerate unit (see Section 4.1.6.) near the headwaters of Takwahoni Creek. The Chuunk volcanic tuff sample was dated by Chemical Abrasion Thermal Ionization Mass Spectroscopy (CA-TIMS, Fig. 17) and detrital zircons from the sandstones were analyzed by the Sensitive High Resolution Ion Microprobe (SHRIMP, Fig. 18).

6.1. Methods

6.1.1. CA-TIMS

CA-TIMS procedures described here are modified from Mundil et al., (2004), Mattinson (2005) and Scoates and Friedman (2008). After rock samples have undergone standard mineral separation procedures zircons were handpicked in alcohol. The clearest, crack- and inclusion-free grains were selected, photographed and then annealed in quartz glass crucibles at 900˚C for 60 hours. Annealed grains were transferred into 3.5 mL PFA screwtop beakers, ultrapure HF (up to 50% strength, 500 mL) and HNO_3 (up to 14 N, 50 mL) were added and caps were closed finger tight. The beakers were placed in 125 mL PTFE liners (up to four per liner) and about 2 mL HF and 0.2 mL HNO_3 of the same strength as acid within beakers containing samples were added to the liners. The liners were then slid into stainless steel Parr™ high pressure dissolution devices, which were sealed and brought up to a maximum of 200˚C for 8-16 hours (typically 175˚C for 12 hours). Beakers were removed from liners and zircon was separated from leachate. Zircons were rinsed with >18 MΩ.cm water and subboiled acetone. Then 2 mL of subboiled 6N HCl was added and beakers set on a hotplate at 80˚-130˚C for 30 minutes and again rinsed with water and acetone. Masses were estimated from the dimensions (volumes) of grains. Single grains were transferred into clean 300 mL PFA microcapsules (crucibles), and 50 mL 50% HF and 5 mL 14 N HNO_3 were added. Each was spiked with a $^{233\text{-}235}U\text{-}^{205}Pb$ tracer solution (EARTHTIME ET535), capped and again placed in a Parr liner (8-15 microcapsules per liner). HF and nitric acids in a 10:1 ratio, respectively, were added to the liner, which was then placed in Parr high-pressure device, and dissolution was achieved at 240˚C for 40 hours. The resulting solutions were dried on a hotplate at 130˚C, 50 mL 6N HCl was added to microcapsules and fluorides were dissolved in high-pressure Parr devices for 12 hours at 210˚C. HCl solutions were transferred into clean 7 mL PFA beakers and dried with 2 mL of 0.5 N H_3PO_4. Samples were loaded onto degassed, zone-refined Re filaments in 2 mL of silicic acid emitter (Gerstenberger and Haase, 1997).

Isotopic ratios were measured a modifed single collector VG-54R or 354S (with Sector 54 electronics) thermal ionization mass spectrometer equiped with analogue Daly photomultipliers. Analytical blanks were 0.2 pg for U and up to 1 pg for Pb. U fractionation was determined directly on individual runs using the EARTHTIME ET535 mixed $^{233\text{-}235}U\text{-}^{205}Pb$ isotopic tracer and Pb isotopic ratios were corrected for fractionation of 0.25%/amu, based on replicate analyses of NBS-982 reference material and the values recommended by Thirlwall (2000). Data reduction employed the Excel-based program of Schmitz and Schoene (2007). Standard concordia diagrams (Fig. 17a) were constructed and regression intercepts, weighted averages

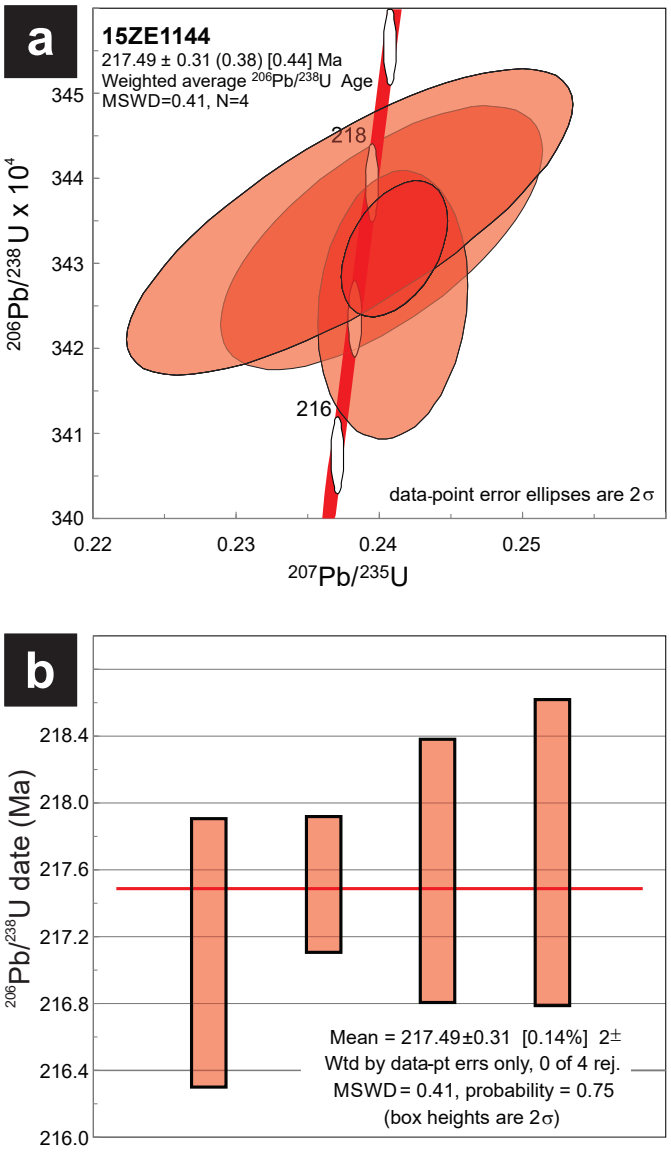

Fig. 17. CA-TIMS geochronology results for sample 15ZE1144, lapilli tuff from Chuunk Mountain. **a)** Concordia plot showing concordant analyses from four grains at 217.49 ±0.31 Ma (weighted average $^{206}Pb/^{238}U$ age). **b)** Statistical treatment of the four analyses.

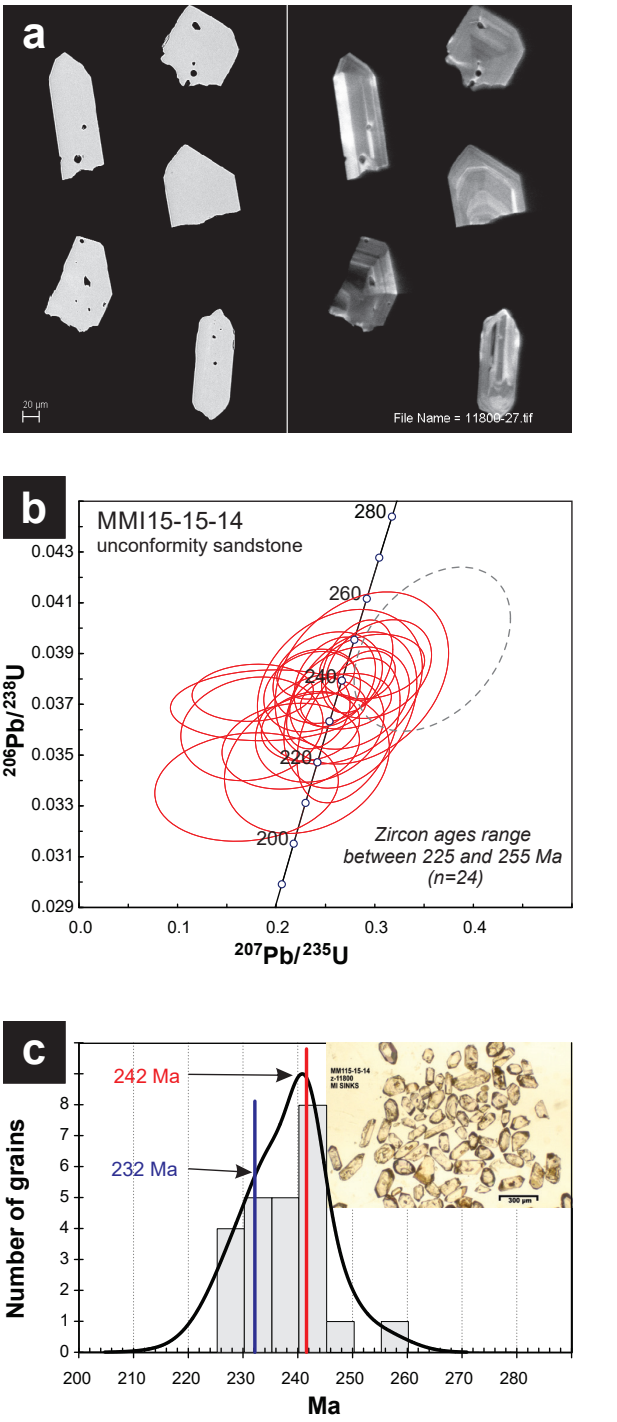

Fig. 18. SHRIMP geochronology results for sample MMI15-15-14, quartz-rich sandstone unconformably below the limestone block conglomerate unit near the headwaters of Takwahoni Creek. **a)** Back-scattered electron mode (left) and cathodoluminescence mode (right) images of a subset of grains analyzed (Scale bar is 20µm). **b)** Concordia plot of the entire set of grains analyzed. The grey dotted ellipse is discordant and not included in age calculations. **c)** age distribution plot: histogram and two age populations resolved using Unmix function in Isoplot 3.00 (Ludwig, 2003). Populations of 232 Ma (blue line) and 242 Ma (red line) are suggested using this function. The youngest grain was 225 ±4 Ma. Inset photomicrograph in transmitted, plane polarized light shows the character of zircons analyzed.

calculated with Isoplot (Ludwig, 2003). Unless otherwise noted all errors are quoted at the 2σ or 95% level of confidence (Table 1). Isotopic ages were calculated with the decay constants l238=1.55125E-10 and l235=9.8485E-10 (Jaffey et al., 1971). EARTHTIME U-Pb synthetic solutions were analyzed on an on-going basis to monitor the accuracy of results.

6.1.2. SHRIMP

Zircon separates for sandstone sample MMI15-15-14 were prepared by standard crushing, disk mill, Wilfley™ table, and heavy liquid techniques. Mineral separates were sorted by magnetic susceptibility using a Frantz™ isodynamic separator. Zircons were analyzed on a mount using the SHRIMP at

Table 1. TIMS analytical results for U-Th-Pb abundance and isotopic composition of zircons from sample 15ZE1144.

		Compositional Parameters								Radiogenic Isotope Ratios								Isotopic Ages					
Sample	Wt. mg	U ppm	Pb ppm	Th/U	$^{206}Pb^*$ x10^{-13} mol	mol % $^{206}Pb^*$	Pb^*/Pb_c	Pb_c (pg)	$^{206}Pb/^{204}Pb$	$^{208}Pb/^{206}Pb$	$^{207}Pb/^{206}Pb$	% err	$^{207}Pb/^{235}U$	% err	$^{206}Pb/^{238}U$	% err	corr. coef.	$^{207}Pb/^{206}Pb$	±	$^{207}Pb/^{235}U$	±	$^{206}Pb/^{238}U$	±
(a)	(b)	(c)	(c)	(d)	(e)	(e)	(e)	(e)	(f)	(g)	(g)	(h)	(g)	(h)	(g)	(h)		(i)	(h)	(i)	(h)	(i)	(h)
15ZE1144																							
B	0.0015	306	10.6	0.272	0.6632	99.01%	29	0.54	1878	0.087	0.051017	1.761	0.240934	1.774	0.034252	0.378	0.140	242	41	219.2	3.5	217.10	0.81
C	0.0017	87	3.7	0.726	0.2072	95.72%	7	0.76	432	0.229	0.050236	5.028	0.237914	5.351	0.034349	0.429	0.769	206	117	216.7	10.4	217.71	0.92
D	0.0010	330	11.5	0.245	0.4828	98.67%	21	0.54	1389	0.079	0.050943	1.187	0.241048	1.254	0.034318	0.192	0.418	238	27	219.3	2.5	217.51	0.41
E	0.0017	73	2.8	0.362	0.1794	96.70%	9	0.50	561	0.116	0.050731	3.587	0.240135	3.821	0.034331	0.369	0.663	229	83	218.5	7.5	217.59	0.79

the Geological Survey of Canada in Ottawa. Analytical procedures and calibration details for the SHRIMP followed those described by Stern (1997) and Stern and Amelin (2003). Briefly, zircons were cast in a 2.5 cm diameter epoxy mount along with the Temora2 zircon primary standard, the accepted $^{206}Pb/^{238}U$ age of which is 416.8 ±0.33 Ma (Black et al., 2004). Fragments of the GSC laboratory zircon standard (z6266, with $^{206}Pb/^{238}U$ age=559 Ma) were also included on the mount as a secondary standard, analyses of which were interspersed among the sample analyses throughout the data session to verify the accuracy of the U-Pb calibration. The mid-sections of the zircons were exposed using 9, 6, and 1 μm diamond compound, and the internal features of the zircons (such as zoning, structures, and alteration) were characterized in both back-scattered electron mode (BSE) and cathodoluminescence mode (CL) using a Zeiss Evo 50 scanning electron microscope (Fig. 18a). The mount surface was evaporatively coated with 10 nm of high purity Au. Analyses were conducted during two separate data sessions, using an ^{16}O- primary beam, projected onto the zircons at 10 kV. Before analysis, the ion beam was rastered over the area of interest for 2 minutes to locally remove the Au coating and eliminate effects of surface common lead. The sputtered area used for analysis was ca. 16 μm in diameter with a beam current of ~7.5 nA. The count rates at ten masses including background were sequentially measured over 6 scans, with a single electron multiplier and a pulse counting system with a deadtime of 20 ns. The 1σ external errors of $^{206}Pb/^{238}U$ ratios reported in the data table incorporate a ±0.80% error in calibrating the standard Temora2 zircon. Age errors reported in the text are at the 2σ uncertainty level, and encompass the combined statistical uncertainty of the weighted mean age for the population and the 2σ error of the mean of the Temora2 zircon calibration standard. Additional details of the analytical conditions and instrument settings are presented in the footnotes of Table 2. Off-line data processing was accomplished using customized in-house software. Isoplot v. 3.00 (Ludwig, 2003) was used to generate concordia plots and to calculate weighted means. Errors for isotopic ratios in Table 2 are given at 1σ uncertainty, as are the apparent SHRIMP ages. No fractionation correction was applied to the Pb-isotope data; common Pb correction used the Pb composition of the surface blank (Stern, 1997). All ages are reported as the ^{207}Pb-corrected weighted mean $^{206}Pb/^{238}U$ age. The error ellipses on the concordia diagram (Fig. 18b) and the weighted mean errors are reported at 2σ.

6.2. Geochronological results

6.2.1. 15ZE1144: Chuunk Mountain volcanic tuff

Four zircons from the Chuunk Mountain tuffaceous rock were analyzed (Table 1). Analyses form a single overlapping population falling on concordia (Fig. 17a) with a weighted $^{206}Pb/^{238}U$ age of 217.49 +0.38/-0.44 Ma (Fig. 17b). This age is considered the best age for the sample.

6.2.2. MMI15-15-14 (Z11800): Quartz-rich sandstone unconformably below limestone block conglomerate unit

Zircons from this sample are large (100-300μm), zoned, and euhedral stubby to semi-elongate prisms (Fig. 18a). Twenty-four grains were analyzed (Fig. 18b). Although most grains have well-preserved facets, ~35% of the grains have subrounded and/or irregular grain boundaries. In transmitted light, the grains are clear and colourless (Fig. 18c, inset), with abundant colourless and brown bubble- and rod-shaped inclusions. In SEM-CL images (Fig. 18a, right), most grains exhibit igneous oscillatory zoning. Approximately 10% of the grains show broad sector zoning. U-Th compositions and U-Th-Pb isotopic ratios of the grains analyzed are shown in Table 2. The grains are generally low in U (39-193 ppm) and low to moderate in Th/U (0.18-0.50). The zircon ages are distributed between 225 and 255 Ma (Figs. 18b, c), with an asymmetric peak at 241 Ma when data are plotted on a conventional probability distribution diagram (not shown). Using the Unmix routine of Isoplot (Ludwig, 2003), the composite peak consists of two possible age populations: 232 Ma and 242 Ma (Fig. 18c). The youngest grain was 225 Ma (grain 100). Two analyses initially yielded younger apparent ages of 217 ±5 Ma (spot 11800-33.1, Table 2) and 220 ±7 Ma (spot 11800-11.1, Table 2). However, replicate analyses on grains 33 and 11 yielded ages of 232 and 238 Ma, respectively, which are indistinguishable from the main populations.

7. Deformation

7.1. King Salmon fault and Whitehorse trough fold and thrust belt

In the Tulsequah area, King Salmon fault is delineated by the main body of Sinwa Formation limestone in its immediate hangingwall as recognized by Souther (1971) who called it the "King Salmon Thrust" (and "King Salmon thrust fault"). Closer to Dease Lake (Fig. 2), Monger and Thorstad (1978) referred to it as the "King Salmon Fault"; and this more generic name is preferred because of evidence for a significant strike-slip

Table 2. SHRIMP U-Pb zircon results for sample MMI15-15-14.

Spot name	U (ppm)	Th (ppm)	Th/U	$^{206}Pb^*$ (ppm)	$^{208*}Pb/^{206*}Pb$	±	$^{238}U/^{206}Pb$	±	$^{207}Pb/^{206}Pb$	±	$^{207*}Pb/^{235}U$	±	$^{206*}Pb/^{238}U$	±	Corr Coeff	$^{207*}Pb/^{206*}Pb$	±	Apparent Ages (Ma) 204 corrected $^{206}Pb/^{238}U$	±	207 corrected $^{206}Pb/^{238}U$	±
Sample Number: MMI15-15-14 - Takwahoni Formation sandstone (NAD83 Zone 8: 592039 E 6525006 N)																					
11800-033.1[a]	*48*	*8*	*0.18*	*1.48*	*0.0587*	*0.0250*	*29.234*	*0.719*	*0.0490*	*0.0033*	*0.1688*	*0.03823*	*0.0337*	*0.0009*	*0.1*	*0.0363*	*0.0082*	*214*	*5*	*217*	*5*
11800-011.1[a]	*62*	*14*	*0.24*	*0.72*	*0.0548*	*0.0173*	*28.653*	*0.930*	*0.0542*	*0.0055*	*0.2299*	*0.03438*	*0.0346*	*0.0011*	*0.2*	*0.0481*	*0.0070*	*220*	*7*	*220*	*7*
11800-100.1	92	27	0.31	1.34	0.0852	0.0194	27.938	0.523	0.0553	0.0026	0.2135	0.02865	0.0353	0.0007	0.1	0.0439	0.0058	224	4	**225**	**4**
11800-032.1	67	22	0.34	-0.33	0.1019	0.0156	27.920	0.906	0.0522	0.0028	0.2726	0.02142	0.0359	0.0012	0.4	0.0550	0.0039	228	7	**226**	**7**
11800-009.1	61	23	0.38	0.71	0.1152	0.0202	27.554	0.654	0.0549	0.0031	0.2433	0.02679	0.0360	0.0009	0.2	0.0490	0.0053	228	5	**229**	**5**
11800-031.1	102	28	0.28	0.67	0.0755	0.0139	27.508	0.415	0.0525	0.0023	0.2335	0.02040	0.0361	0.0006	0.2	0.0469	0.0040	229	3	**230**	**3**
11800-033.2	57	11	0.21	-0.47	0.0839	0.0171	27.342	0.934	0.0502	0.0033	0.2743	0.02766	0.0367	0.0013	0.3	0.0541	0.0051	233	8	**232**	**8**
11800-018.1	73	23	0.33	1.38	0.0834	0.0195	27.391	0.616	0.0469	0.0024	0.1741	0.02967	0.0360	0.0008	0.1	0.0351	0.0059	228	5	**232**	**5**
11800-099.1	187	71	0.39	0.45	0.1011	0.0100	27.182	0.425	0.0517	0.0016	0.2418	0.01325	0.0366	0.0006	0.3	0.0479	0.0025	232	4	**233**	**4**
11800-017.1	96	33	0.35	0.45	0.1109	0.0146	26.833	0.315	0.0565	0.0024	0.2697	0.01888	0.0371	0.0005	0.2	0.0527	0.0036	235	3	**234**	**3**
11800-106.1	122	43	0.36	0.73	0.0955	0.0138	26.664	0.586	0.0595	0.0035	0.2735	0.02492	0.0372	0.0008	0.2	0.0533	0.0047	236	5	**235**	**5**
11800-011.2	68	25	0.38	1.45	0.0822	0.0225	26.677	0.365	0.0499	0.0048	0.1905	0.04073	0.0369	0.0006	0.1	0.0374	0.0080	234	4	**238**	**3**
11800-027.1	78	22	0.30	0.65	0.0851	0.0173	26.372	0.866	0.0562	0.0050	0.2635	0.03437	0.0377	0.0012	0.3	0.0507	0.0064	238	8	**238**	**8**
11800-001.1	106	21	0.21	0.75	0.0762	0.0138	26.484	0.450	0.0519	0.0021	0.2354	0.02014	0.0375	0.0007	0.2	0.0455	0.0038	237	4	**239**	**4**
11800-019.1	39	7	0.18	0.60	0.0514	0.0196	26.148	0.945	0.0596	0.0042	0.2861	0.03615	0.0380	0.0014	0.3	0.0546	0.0066	241	9	**240**	**9**
11800-005.1	174	64	0.38	-0.24	0.1310	0.0103	26.297	0.273	0.0533	0.0017	0.2907	0.01199	0.0381	0.0004	0.3	0.0553	0.0022	241	2	**240**	**3**
11800-101.1	90	23	0.27	0.24	0.0913	0.0129	26.339	0.500	0.0516	0.0024	0.2588	0.01697	0.0379	0.0007	0.3	0.0496	0.0031	240	5	**240**	**5**
11800-008.1	72	26	0.38	0.31	0.1183	0.0178	25.979	0.537	0.0599	0.0030	0.3031	0.02202	0.0384	0.0008	0.3	0.0573	0.0040	243	5	**241**	**5**
11800-071.1	150	50	0.34	1.04	0.0696	0.0134	26.015	0.494	0.0567	0.0022	0.2512	0.02281	0.0380	0.0007	0.2	0.0479	0.0042	241	5	**242**	**5**
11800-007.1	141	67	0.50	1.78	0.1062	0.0160	26.234	0.295	0.0492	0.0018	0.1747	0.02527	0.0374	0.0005	0.1	0.0338	0.0049	237	3	**242**	**3**
11800-035.1	53	12	0.24	-0.34	0.1011	0.0156	26.084	0.343	0.0531	0.0029	0.2968	0.02185	0.0385	0.0005	0.2	0.0560	0.0040	243	3	**242**	**3**
11800-037.1	135	49	0.38	0.29	0.1212	0.0116	25.915	0.502	0.0555	0.0019	0.2814	0.01482	0.0385	0.0008	0.4	0.0530	0.0026	243	5	**243**	**5**
11800-015.1	193	62	0.33	0.84	0.0992	0.0112	25.976	0.263	0.0526	0.0016	0.2391	0.01608	0.0382	0.0004	0.2	0.0454	0.0030	241	3	**243**	**2**
11800-012.1[b]	*52*	*18*	*0.36*	*-0.77*	*0.1378*	*0.0217*	*25.732*	*0.862*	*0.0599*	*0.0034*	*0.3580*	*0.03254*	*0.0392*	*0.0013*	*0.4*	*0.0663*	*0.0056*	*248*	*8*	*243*	*8*
11800-013.1	71	23	0.33	-0.59	0.1133	0.0163	25.851	0.627	0.0516	0.0050	0.3031	0.03337	0.0389	0.0010	0.2	0.0565	0.0061	246	6	**245**	**6**
11800-016.1	127	41	0.34	0	0.1108	0.0105	25.587	0.400	0.0507	0.0019	0.2732	0.01120	0.0391	0.0006	0.4	0.0507	0.0019	247	4	**247**	**4**
11800-103.1	77	32	0.44	-1.01	0.1667	0.0180	24.765	0.501	0.0511	0.0025	0.3344	0.02806	0.0408	0.0009	0.2	0.0595	0.0048	258	5	**255**	**5**

Notes (see Stern, 1997):

Mount IP824, K100b spot size (13x16µm), 2 minute raster, 6 mass scans

Primary beam intensity ~7.5nA,Weighted mean 207Pb-corrected 206Pb/238U age of the analyses of secondary standard z6266 zircon was determined to be 558 ± 8 Ma, MSWD=1.4, n=25 (2 rejections) (accepted 206Pb/238U age is 559 Ma)

Spot name follows the convention x-y.z; where x = lab number, y = grain number and z = spot number

Uncertainties reported at 1s and are calculated by using SQUID 2.50.11.10.15, rev. 15 Oct 2011

204Pb and f(206)204 are not reported here due to space limitations. For complete data set please contact the corresponding author.

* refers to radiogenic Pb (corrected for common Pb)

Calibration standard Temora2; Age = 416.8 +/-0.33 Ma (Black et al., 2004)

Error in 206Pb/238U calibration 0.80% (included)

Standard Error in Standard calibration was 0.72% (not included in above errors but required when comparing data from different mounts).

Apparent ages shown in bold font are those which were included in weighted mean age calculations

bdl : below detection limit

a: indicates an analysis that was younger than other grains in the sample, but a second replicate analysis yielded a result that was indistunguishable from the older population

b: analysis was discordant and thus not included in any age interpretation

component. Although many regional scale maps portray the King Salmon fault as single southwest-verging strand, Souther (1971) identified an additional thrust strand southwest of what he mapped as the main fault trace. This strand extends from the headwaters of King Salmon Creek, where it carries Stunini Group sedimentary rocks, to near its confluence with the Taku River, northwest of which it rapidly dies out into the contact between "Sinwa Formation" and underlying Triassic strata.

In agreement with Souther (1971), our mapping in the Sinwa Creek area delineated more than one thrust fault carrying Sinwa Formation strata southwest over undated, but presumably younger rocks. However numerous thrust faults appear to cut and thicken the Sinwa Formation internally and repeat less distinctive strata in both the hangingwall and footwall of the King Salmon fault (Figs. 3, 19). Hence the King Salmon fault is just one of many faults comprising a regionally extensive fold and thrust belt mapped in the area (English et al., 2005) and to the northwest (Mihalynuk et al., 1999), which we herein call the 'Whitehorse trough fold and thrust belt'. Earlier works also documented thrust faults in the Laberge Group (e.g., Souther, 1971; and in Yukon, Wheeler, 1961), but the thrust shortening implied by this work is not as great as that suggested by more recent work in Yukon (e.g., Colpron, 2011) and northernmost BC (Mihalynuk et al., 1999). In the Sinwa Creek area, most of the regional and mountain scale fold hinges parallel the King Salmon fault and other faults in the Whitehorse trough fold and thrust belt, but a sparsely developed fold set displays steeply plunging hinges (Fig. 20).

Early Middle Jurassic deformation in the Whitehorse trough was protracted, (Mihalynuk et al., 2004), starting from the Cache Creek in the northeast and migrating southwest toward Stikine terrane. This deformation has been attributed to oblique (dextral, south-southwest) overthrusting of Cache Creek above Stikine terrane as extrapolated from the Dease Lake area (Fig. 21b; Mihalynuk et al., 1999). However, Whitehorse trough fold and thrust belt fold orientations in the Sinwa Creek area indicate more west-directed shortening direction (Fig. 21a), and a less obvious geometric and kinematic link to dextral offset on the Llewellyn fault zone. In addition, steeply plunging folds with hinges nearly orthogonal to the fold belt (Figs. 20, 21a) are unlikely to have been formed by dextral oblique underthrusting.

7.2. Steep fold hinges

Outcrop- to mountain-scale folds of the Sinwa Formation in the hangingwall of the main strands of the King Salmon fault (Fig. 19) locally display hinges that plunge steeply northeast and axial surfaces that dip southeast (Figs. 20, 21a). Within these folds, fossils as strain markers show one of three characteristics: no deformation, flattening parallel to the fold axial surfaces (uncommon), or bedding-parallel flattening within hinge zones of concentric folds (Fig. 20b). Conglomerate clasts show the same strain characteristics. West of Sinwa Mountain peak, the core of one such steep fold is exposed in outcrops of intrusive boulder conglomerate scattered over an area of about 10 m^2 (Fig. 19c). Strain gradients are high. Within a few metres, undeformed, subround cobbles pass into strongly flattening clasts displaying width-to-thickness ratios of >8. This clast flattening is concentrated in the steeply plunging concentric fold hinge (e.g., 354°/62°-90°). Similar folds are observed in the footwall strata, including sandstone (Fig. 20 a) and intrusive cobble conglomerate. The relationship of the steep folds to the main phase of shortening in the Whitehorse trough fold and thrust belt is unknown. Although some steep fold limbs appear to be truncated by thrust faults (Fig. 21a), sense of motion on these faults has not been determined unequivocally. Regardless of relative timing of the thrusts and steep folds, the steep fold hinge plane orientations are consistent with a sinistral, not dextral component of oblique motion in the fault zone. Implied sense of motion is lower plate southward relative to the upper plate, opposite of that expected of south- or southwestward-directed thrusting (Figs. 2, 21).

8. Discussion

Our primary aim was to address the nature of the King Salmon fault and its effect on the Late Triassic-Early Jurassic porphyry deposits that track northwards through BC into the Yukon. Our mapping in the Sinwa Creek mapsheet relied heavily on rapid field data collection techniques and remote imagery; it does not conform to BC Geological Survey 1:50,000-scale map data coverage standards. Some fossil identifications and isotopic age determinations are pending and detailed sections and age control that are necessary to conclusively constrain structural duplication are currently lacking. Although much of the area falls within the 805 km^2 Taku River conservancy and adjacent 1673 km^2 Nakina-Inklin River conservancy (Figs. 2, 3) established in 2012, the Sinwa Creek area occupies a pivotal position to understanding the regional geological history and mineral potential in adjacent areas. It is here that the King Salmon fault is best exposed and associated deformation is most apparent, and so it is likely the best place to constrain the degree of overthrusting and tectonic burial of the Late Triassic-Jurassic porphyry belts.

8.1. King Salmon fault

Expression of the King Salmon fault in the Sinwa Creek area, where it carries Sinwa Formation in its hangingwall, contrasts with the fault expression in the eastern Dease Lake and Cry Lake areas, where its trace is defined by lenses of serpentinized peridotite and chert in the hangingwall (Fig. 2; Gabrielse, 1998; Monger and Thorstad, 1978). Such contrast in crustal level of the hangingwall begets the question: Are these the same fault? The amount of shortening, the crustal level of the thrust sole, the possibility of different basement to the Whitehorse Trough in these two regions, and the uncertainty in the Stikinia – Cache Creek terrane boundary location are all considerations.

8.1.1. Amount of overthrusting

The Triassic arc narrows from >250 to <10 km between 58.5°N and the BC-Yukon border (60°N) suggesting either: structural excision to the west along the Llewelyn fault, burial

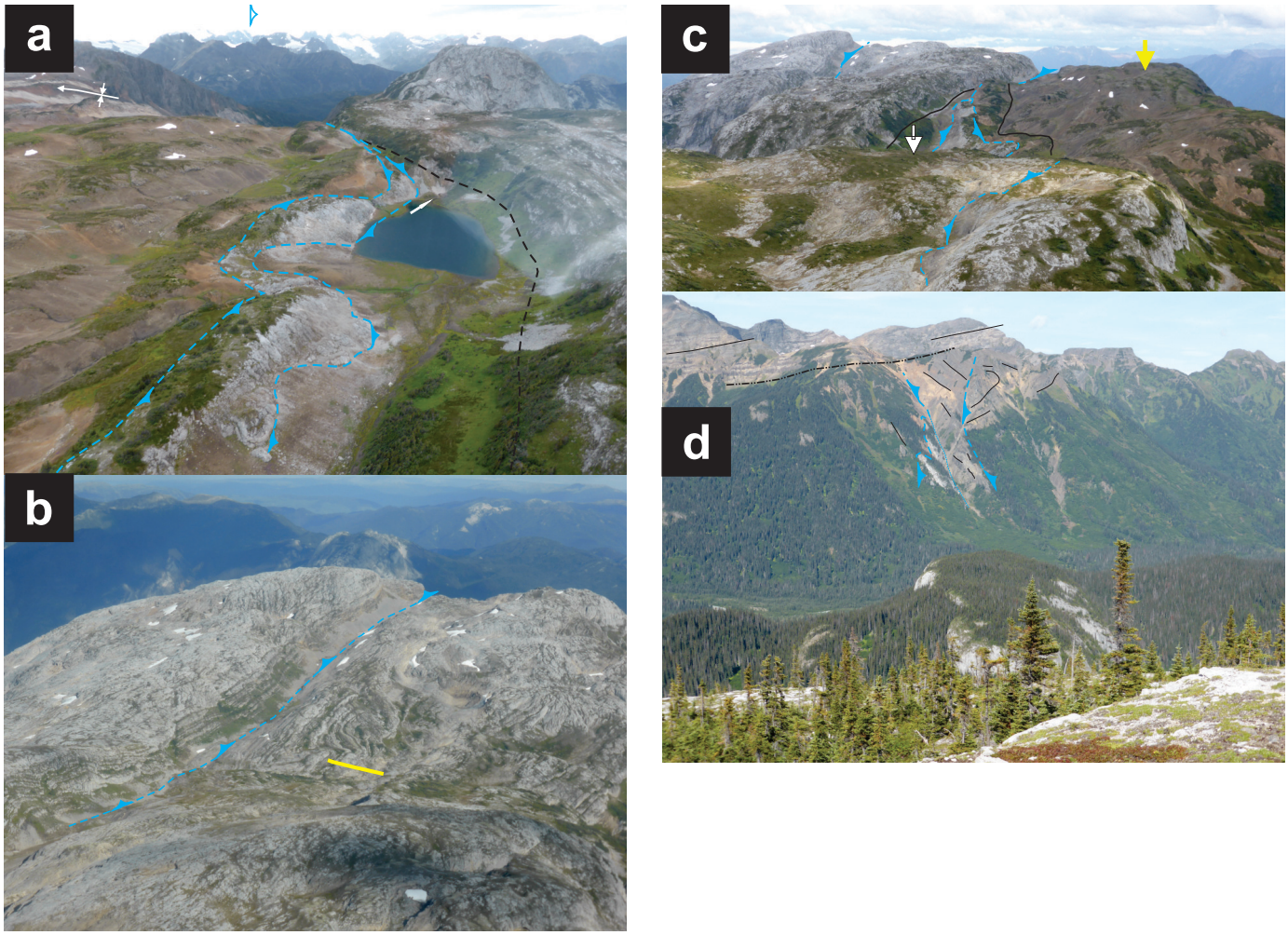

Fig. 19. a) View northwest along the leading edge of the main Sinwa Fm. limestone which is interpreted as the hangingwall of the principal strand of the King Salmon Fault. A karst lake sits mainly atop black argillite that forms the valley bottom toward the photographer and drains into a limestone cavern to the northeast (white arrow). A thin limestone layer between the black argillite and an orange-weathering, broken argillite and siltstone unit is interpreted as a separate thrust sheet. **b)** View southeast along the Sinwa Fm. limestone from near Sinwa Mountain. Strata southwest of the valley (occupied by blue thrust symbols) display significant shortening, in sharp contrast to strata to the northeast which dip steeply, but are not significantly folded, indicating that a detachment surface (thrust) occupies the valley. Yellow line shows the approximate location of a section sampled in 2016 for conodont biogeochronology. **c)** View to the southeast along the King Salmon Fault zone. Blue barbed lines outline faults shown in a and b. White arrow point to karst lake of Figure 19a hidden behind near horizon. Black lines are the approximate contacts between recessive black shale and limestone to the left (northeast) and, to the right, between orange weathering argillaceous siltstone and wacke and intrusive conglomerate unit of Figs. 5b, c. Yellow arrow show the approximate location of a steep fold hinge within the boulder conglomerate where hinges defined by flattened and folded clasts measure 354°/62° to nearly vertical. **d)** view to the north-northwest of the northern termination of the main belt of Sinwa Fm. limestone. Solid black lines highlight layering. A considerable thickness of light grey Sinwa Fm. in foreground terminates in gully to north, apparently truncated by a thrust that cuts up section through footwall and hangingwall strata (thrusts shown by blue dashes with barbs in hangingwall; dotted blue is interpreted stratigraphic top of the Sinwa Fm.). The hangingwall is interpreted to be cut by another thrust that is overturned as it cuts up section and carries an overturned antiform, probably also cored by a thrust (not shown). Sloko Group volcanic strata unconformably overlie the thrust panels (unconformity approximated by black dash, double dot) and gently dip to the west.

by the Jurassic strata of the Whitehorse trough, or significant overthrusting along the King Salmon fault. The King Salmon fault in the Sinwa Creek area has significant apparent offset because the ~70 m-thick carbonate-cream chert with over- and underlying boulder conglomerate in the footwall of the fault contrasts strongly with the hundreds of metres-thickness of main carbonate and underlying petroliferous silty mudstone at Sinwa Mountain. Intervening fault panels with carbonate rocks of intermediate thickness and underlying clastic strata with intermediate grain size are lacking. If the cream chert is correlative with the main belt of Sinwa Formation, then transitional faces have been overthrust to juxtapose distinct facies. However, it is possible that the chert unit and main carbonate unit did not originate as widely separated facies, limiting the need for significant bedding-parallel shortening for their juxtaposition. In order to quantify the amount of

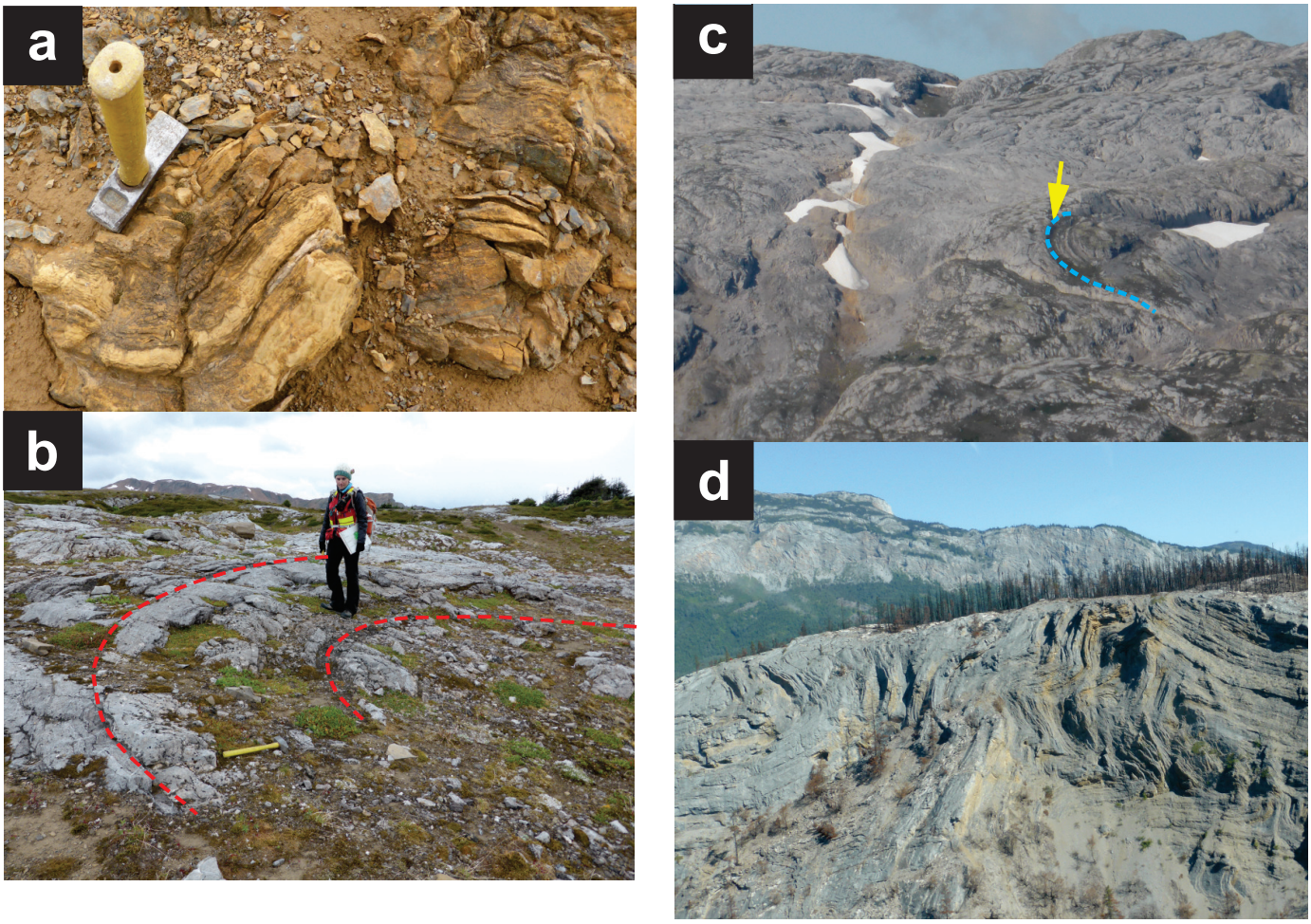

Fig. 20. Moderately plunging to vertical fold hinges occur at all scales within and near the Sinwa Formation. **a)** About 2 km within the footwall of the King Salmon fault, steeply plunging folds in calcareous sandstone (fold hinge is approximately parallel to the hammer handle). **b)** View to the south of a nearly vertical fold hinge outlined by beds of fossiliferous Sinwa Formation limestone. This fold appears to be cylindrical, with a hinge trending ~015°/85°. **c)** dark, argillaceous strata are cut along a fault outlined by snow patches, and in the centre of the photo a steeply-plunging fold is well displayed. **d)** Views of Sinwa Formation limestone cliffs from south of the Taku River northward to the south flank of Sinwa Mountain (in distance, north of the Taku River). Fold hinges plunge moderately to the northeast and folds verge northwest, suggest transport oblique to the regional trace of the King Salmon fault.

overthrusting, the stratigraphy of hangingwall and footwall sections and structural cut-offs need to be established. If previous workers who have suggested a forearc setting for the Whitehorse Trough are correct, then estimates for original facies distributions can be guided by modern oceanic forearc environments. For example, the Sunda arc, which forms above the subducting oceanic lithosphere of the Australian plate, and extends for >6000 km. Along its length, forearc basins between the magmatic arc and outer-arc ridge are 50-100 km wide and segmented into sub-basins ~100 km long (Van der Werff, 1996). West of central Sumatra, the forearc basin shelf is underlain by two shallow water carbonate successions 700-800 m thick separated by a ~200 m coaly volcanic conglomerate and tuffite facies that was deposited during a Miocene lowstand (Beaudry and Moore, 1981). The upper carbonate succession is coralgal detrital limestone deposited from upper Pliocene to present. Relatively clean carbonate is able to accumulate because the basin has continually subsided, resulting in the trapping of arc-derived clastics near the un-filled basin margin, except for the Middle Miocene. Based on seismic stratigraphy, juxtaposition of Sunda arc coarse clastic facies with carbonate bank deposits might only require ~10 km of overthrusting, consistent with the 16 km minimum estimate of King Salmon fault overthrusting based on an interpreted klippe of Sinwa Formation. east of Trapper Lake (Fig. 2; Souther, 1971).

8.1.2. Boundary of the Cache Creek terrane?

Souther's mapping and interpretation of the King Salmon fault predated the mobilist framework of plate tectonics (e.g., Vine and Hess, 1970), identification of the exotic nature of the Cache Creek terrane (Coney et al., 1980; Monger, 1975), and quantitative estimates of the huge horizontal displacements along plate margins (e.g., Kreemer et al., 2014; Sigloch and Mihalynuk, 2013). Mobilist notions helped to

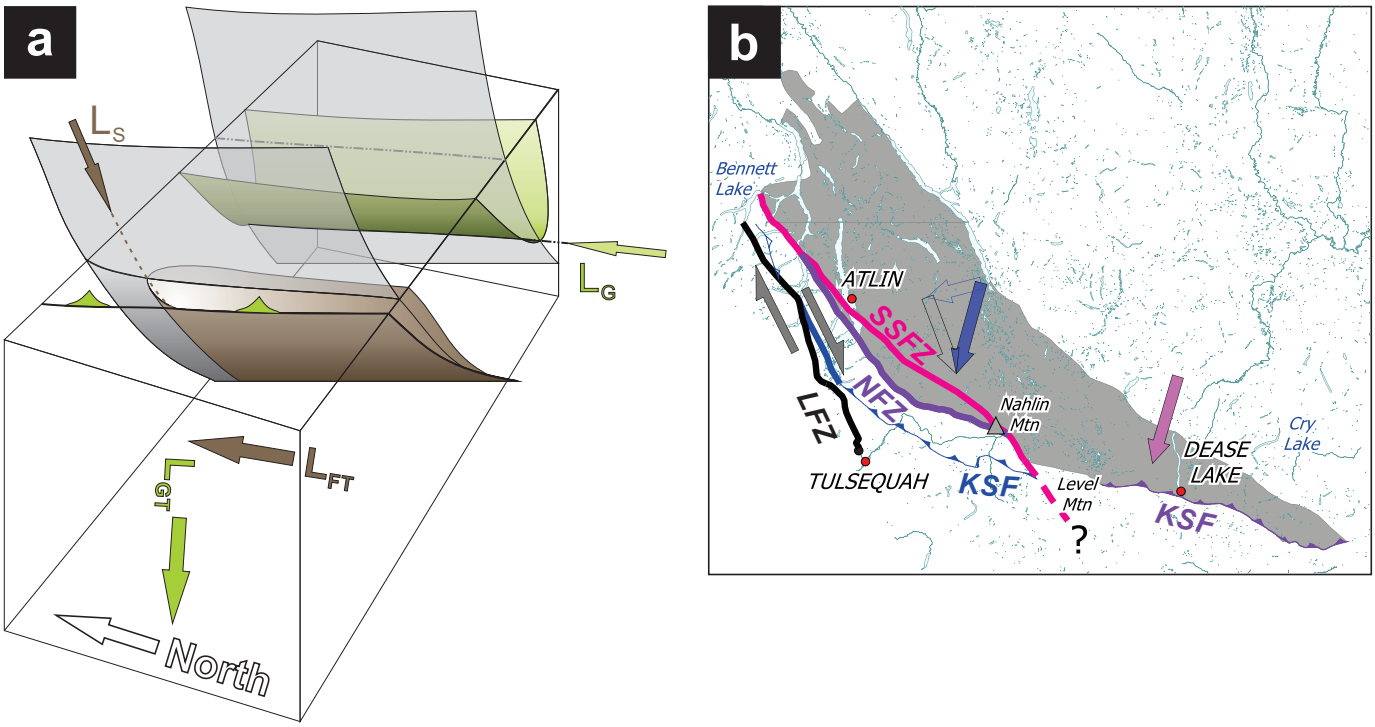

Fig. 21. a) Block diagram representation of the sparse steeply plunging fold lineations (L_S, brown) in comparison with the typical gently plunging fold lineations (L_G, green) and thrust faults (with green barbs) of the Whitehorse trough fold and thrust belt. Interpreted transport directions during formation of the gentle (L_{GT}) and steep (L_{FT}) folds are shown. In this representation, the thrust is interpreted to cut the L_S fold at depth, but such a relationship has not yet been observed (e.g., outlasts L_{FT} deformation). Nevertheless, if the L_S fold is restored to a pre-L_G orientation it verges northerly (axial surface dips southerly). **b)** Geometry of major faults in northwestern British Columbia modified after Mihalynuk et al. (1999). Convergence vectors were extrapolated from those unambiguously determined in the Dease Lake area (purple vector) and assumed to be consistent across the northern Cache Creek terrane. North over south transport on the southern portion of the Nahlin fault zone (NFZ) was interpreted to change northward to predominantly dextral motion as the fault orientation changes. So too for the King Salmon fault as it converges with the Llewellyn fault zone (LFZ) north of Atlin Lake, where strike slip motion is dominant. Components of convergence that are parallel and normal to the Llewellyn fault zone are shown by the black and blue vector outlines. Although major folds and faults parallel the King Salmon fault, steep folds within the thrust sheets are consistent with a sinistral, not dextral component of motion during, or immediately before thrusting (see Discussion).

formulate the tectonic assemblage and terrane maps of the Canadian Cordillera, which show the King Salmon thrust as the southwestern boundary of the Cache Creek terrane, and as such, a suture zone (Wheeler and McFeely, 1991; Wheeler et al., 1988). However, various lines of evidence argue against the King Salmon fault forming the southwest boundary of the oceanic Cache Creek terrane. Some of the strongest evidence is that correlatives of the Sinwa Formation, which mark the hangingwall of the King Salmon fault, are in stratigraphic contact with Stikine terrane rocks between Atlin Lake and 60° N (Wight et al., 2004; Mihalynuk and Mountjoy, 1990) and farther north, in Yukon (e.g., Wheeler, 1961; Colpron, 2011). In addition, the Takwahoni facies of the Laberge Group occur in both the footwall and hanging wall of the King Salmon fault, suggesting that the fault juxtaposes different facies of the same basin(s) rather than bounding terranes. North of Nahlin Mountain, the absence of any exotic rock types along the King Salmon fault, or its splays, is consistent with it rooting at the base of the Sinwa Formation or in underlying argillaceous strata, rather than in the exotic Cache Creek terrane (with the possible exception of the quartz-rich sandstone with unmixed age population of ~242 Ma detrital zircons; see above). In addition, Cache Creek did not appear to contribute detritus throughout the Early Jurassic evolution of the Whitehorse trough and was either tectonically or stratigraphically buried or geographically isolated during the Early Jurassic.

8.1.3. Shared identity at fault

Unlike the Sinwa Creek-Tulsequah area, the King Salmon thrust in the eastern Dease and Cry Lake areas (Fig. 2) is marked by Cache Creek terrane rocks in the hangingwall. The difference between the nature of the thrust in these areas may be explained in two ways.

The first explanation is that the King Salmon fault in these areas represents two fundamentally different faults. Accordingly, in the Dease and Cry Lake areas it is a crustal-scale fault that carries Cache Creek terrane mantle in the hanging wall and roots into the Nahlin fault south of Nahlin Mountain; whereas in the Sinwa Creek-Tulsequah area, it belongs to a thin-skinned thrust belt where it carries Sinwa Formation in its hangingwall

for about 90km, forming an almost unbroken limestone belt centred on King Salmon Lake (Fig. 2).

The second explanation is that the King Salmon and Nahlin faults form two major loci of Middle Jurassic displacement in the same thrust and fold belt, which imbricates a Latest Triassic-Middle Jurassic Stikinia-Cache Creek suture that was overlapped by the Whitehorse trough. Implicit in this explanation is that the Cache Creek terrane formed incrementally, as many accreted microterranes, atop of which the Late Triassic forearc of the Stikine terrane was locally constructed. Both of these explanations involve changes in the composition of the hangingwall across a curious appendage of Cache Creek terrane southeast of Nahlin Mountain (Fig. 2) that extends into the Whitehorse Trough. The idea that the boundary of the Cache Creek terrane changes from the Nahlin fault northwest of Nahlin Mountain, to the KSF to the southeast has been incorporated into the terrane map of Colpron and Nelson (2011), but evaluation of alternate explanations for this change will require mapping the remote areas southeast of Nahlin Mountain and in the Cry Lake areas. Regardless of the nature of the mode of Cache Creek – Whitehorse Trough juxtaposition, reconnaissance investigations as part of GEM indicate significant modification of the contact by transcurrent faulting (Zagorevski, unpublished data).

8.2. Regional fault network and kinematics

Northward projection of the King Salmon fault connects it with the crustal-scale Llewellyn fault zone (Figs. 2, 21b; Bultman, 1979; Mihalynuk et al., 1999; see also discussion in Wight et al., 2004). Assumed south(west)ward thrusting of the King Salmon fault is consistent with its overall thrust fault geometry and orientation, paralleled by major folds that can be traced for kilometres. All suggest a kinematic link with late dextral motion on the Llewellyn fault zone (Mihalynuk et al., 1999). Inconsistent with such a link are outcrop to mountain-scale folds within thrust panels that have moderate to steeply northeast-plunging fold hinges and southeast dipping axial surfaces, pointing to a sinistral, not dextral component of motion along the King Salmon fault (Fig. 21a, see above). An alternative explanation for steep fold axes is strongly inhomogeneous transport of previously developed hinge lines in the direction of thrusting, but ductile fabrics supporting such flow are lacking. Polyphase deformation is another possible explanation for the steep hinges, but clear evidence of refolding of early structures has not been observed, and flattening fabrics, which seem largely confined to the steep fold hinges, likely developed during progressive, rather than polyphase, deformation. Observations from these sparsely developed, steeply plunging folds are not sufficiently numerous to warrant statistical treatment and key crosscutting relationships have not been observed. Their significance is still poorly understood, but they appear to indicated a phase of sinistral strain in the Whitehorse trough fold and thrust belt, the relative timing of which is not constrained.

North of Atlin Lake, the King Salmon fault is interpreted to join the dextral Llewellyn fault (Figs. 2, 21b), which separates the Whitehorse Trough from metamorphosed rocks to the west. West of the junction, metamorphic rocks include the strongly deformed Hale Mountain granodiorite (Mihalynuk and Mountjoy, 1990), a K-feldspar augen gneiss which is part of the Aishihik plutonic suite (Fig. 2; Woodsworth et al., 1992; Johnston et al., 1996). The gneissic fabric is steep, penetrative, pervasively affects the granodiorite and displays sinistral shear sense indicators (Mihalynuk et al., 1999). It is crosscut by an aplitic dike swarm that is offset by, and locally intrudes, pervasive brittle fractures with dextral offsets. U-Pb zircon crystallization ages of the granodiorite and cross-cutting aplite dikes are 186.5 ±1.5 Ma and 178.8 ±0.9 Ma (Mihalynuk et al., 1999). About 20 km to the south, the ductile fabric overprints a quartz monzodiorite body and is in turn overprinted by metamorphic monazite; the intrusion and monazite are U-Pb dated as 180.9 ±3.1 and 177.5 ±1.5 Ma (Currie, 1994; Currie and Parrish, 1997). It is unknown if the granodiorite and quartz monzonite were intruded into an already active deformation zone, but ductile sinistral shear ceased by ~178 Ma. Immediately following, at ~177 Ma (Currie, 1994), metamorphism peaked at upper amphibolite facies within the metamorphic rocks west of the Llewellyn fault, suggesting tight interdependency.

Sinistral offset related to ductile deformation within the Llewellyn fault zone (older and deeper deformation, which is overprinted by young and shallower, brittle fabrics, (Mihalynuk et al., 1999; Ootes et al., 2017) is suggested by a new, preliminary U-Pb crystallization age of ~185 Ma (Friedman, unpublished) from a 2.5 km-long lens of protomylonitic granodiorite along the Llewellyn fault (Fig. 2) where it crosses southern Tutshi Lake (Mihalynuk et al., 1999). It is possible that this body intruded into the fault near its present location and intrusive contacts were obscured by later deformation, but we suggest that it is a part of the Hale Mountain granodiorite border that was offset sinistrally, by about 70 km.

Sinistral fabrics are also observed within conglomerate facies of the Laberge Group in northernmost BC (Mihalynuk et al., 1999) where fossil age constraints limit deformation age to younger than 183 Ma. Regional constraints on youngest (western) Whitehorse trough fold and thrust belt deformation come from the Tulsequah and Dease Lake areas where Laberge Group strata as young as Bajocian (~170 Ma) and are deformed by nearly syndepositional folds and thrusts (Mihalynuk et al., 1995). Structures correlated with the old eastern Whitehorse trough fold and thrust belt, emplace 174 Ma blueschist along with Cache Creek strata and are cut by 172 Ma intrusions (M. Mihalynuk et al., 2004).

8.3. Disruption during Latest Triassic carbonate deposition

Preservation of carbonate is not solely controlled by depositional facies arising from the interplay of paleogeography, climate, and ocean chemistry. Evolution too plays an important role, especially in Triassic and Jurassic times, when reef forming organisms were recovering from two global extinction crises. During the Permo-Triassic mass extinction event,

carbonate reef-formers were wiped out and did not widely reappear until the Middle Triassic. It was not until the Norian that corals became important reef-formers, especially the Scleractinians (Stanley, 2003; Flügel, 2002). Reef-formers were similarly hard-hit by the end Triassic extinction event and did not rebound until the third stage of the Early Jurassic (Pliensbachian. Stanley, 2003; although rare reefs from the first two Jurassic stages are known, Hodges and Stanley Jr, 2015). As a result of evolution, lack of reefal carbonate accumulation during the Early-Middle Triassic and first half of the Early Jurassic in the Sinwa Creek area does not necessarily indicate inappropriate depositional environment (e.g., too deep) or climate (e.g., too cool).

Against this backdrop, it is not surprising that Sinwa Formation is largely restricted to the Norian. Spatial distribution of Sinwa Formation is from southeast of Sinwa Creek map area to north of Whitehorse, where warm water carbonate reef mounds are fringed by inter-mound carbonate sandstone, as at the well-studied Lime Peak locality (Reid, 1985; Reid and Tempelman, 1987; Yarnell et al., 1998). The Sinwa Formation in these areas are relicts of what was probably a much more widespread reef-mound-sandstone complex before Late Norian uplift and erosion. Latest Triassic uplift of the western side of the Whitehorse Trough between southern Atlin Lake and Yukon is marked by an unconformity developed late during carbonate deposition, roughly synchronous with late arc alkalic volcanism (Mihalynuk et al., 1999; Logan and Mihalynuk, 2014) and predating onset of Laberge Group deposition in Early Jurassic. Within the Sinwa Creek area, this event may be represented by limestone block conglomerates (see above). Widespread occurrence of Norian carbonate and Late Triassic igneous boulders in Late Triassic conglomerate is consistent with exposure of the Sinwa Formation or a similar limestone unit and the underlying Late Triassic Stuhini arc, starting in the Late Triassic as indicated by probable *Halobia* bivalves in strata below the limestone block conglomerate which is inferred to be composed of Late Norian carbonate, like all limestone clasts dated within the Whitehorse trough. The age of strata overlying the unconformity is unknown; although, Souther (1971) reported an Early Toarcian ammonite collected from strata along strike, and in the Stuhini Creek area, volcanic conglomerate is commonly Pliensbachian in age (Mihalynuk et al., 2004; igneous conglomerate is Pliensbachian to Toarcian). North of the Sinwa Creek map area, this period of uplift and exposure may have extended through to the Early Jurassic as recorded by detrital zircons ranging from Late Triassic through Early Jurassic and boulders of Norian carbonate in the Laberge Group (Early Jurassic; Colpron et al., 2015). Southeast of the Sinwa Creek area, Souther (1971) mapped Laberge Group in contact with Stuhini arc strata without intervening Sinwa Formation, and ~80 km southeast of Sinwa Mountain, Laberge Group strata are mapped in stratigraphic contact with Triassic intrusive rocks.

The underlying causes of the Late Norian uplift are not known, but Logan and Mihalynuk (2014) have suggested that collision of the Kutcho-Sitlika arc with the Quesnel-Stikine arc at this time initiated a pulse of alkalic magmatism with high Cu-Au-Ag tenor, and generated economically important porphyry deposits along the length of the province. Such an event may explain the main 242 Ma detrital zircon population (resolved from a 232 Ma subpeak using Unmix routine of Isoplot; Ludwig, 2003) in the strata at the unconformity, a magmatic age unknown in adjacent Stikinia, but predominant in the Kutcho-Sitlika arc (Childe and Thompson, 1995; Mihalynuk et al., 2003; Schiarizza, 2013). Magmatic ages of ~232 Ma are also not known within Stikine terrane; although in the Quesnel arc, felsic magmatism seems to have been underway by ~239 Ma (Mihalynuk et al., 2016) and crystallization ages of 230.2 ±0.8 Ma have been reported (Erdmer et al., 2002). However, it seems unlikely that a unimodal population of zircons could transit from the outer arc ridge collision site to the interior of the pre-collision platform without contamination from other detrital zircon sources. A reassessment of the currently accepted Stikine subduction polarity may be warranted.

Regardless of tectonic model, a widespread unconformity is indicated and implications are that the Stuhini arc was eroded to its plutonic roots between the latest Triassic and Early Jurassic. Consequences for preservation of Late Triassic – Early Jurassic porphyry deposits in these areas would thus appear dire, unless the mineralized arc was tectonically buried during Middle Jurassic collapse of the Whitehorse Trough or decapitated during the Late Triassic arc disruption and preserved at a structural level below the current erosional surface. Careful delineation of the mineralized arc axes will be required before such options can be properly evaluated.

9. Summary

Reconnaissance mapping in the Sinwa Creek map area (104K/14) of northwest British Columbia (59°N) was conducted in 2015 to determine what happens at this latitude to a Triassic-Jurassic magmatic belt that is mineralized with Cu-Au porphyry deposits as far north as ~58.5°. Sinwa Creek map area is mostly underlain by Triassic and Jurassic volcanosedimentary strata of the Whitehorse trough, which parallels the western boundary of the exotic, oceanic Cache Creek terrane in BC and extends along strike into central Yukon (~500 km in total). The area is diagonally bisected by a belt of massive to well-bedded limestone, the Sinwa Formation, that defines the King Salmon fault. At this latitude, the King Salmon fault is a northeast-dipping thrust, part of the Whitehorse trough fold and thrust belt that includes folds recording sinistral transpression. Many previous workers have included the Sinwa (and Whitehorse trough strata northeast of the Sinwa Formation) with the Cache Creek terrane, which lacks known porphyry deposits. We favour an alternative hypothesis, supported by stratigraphic, biochronologic (conodont), clast compositions, detrital zircon populations, and rock types in the immediate hangingwall of the King Salmon fault, which places the Whitehorse trough above the Stuhini forearc. If correct, the King Salmon fault within, or north of, the Sinwa Creek area is not the Cache Creek

terrane boundary. However, southeast of Nahlin Mountain, the King Salmon fault as currently defined **does** carry Cache Creek terrane rocks in its hangingwall, placing Cache Creek terrane and structurally overlying parts of the distal Whitehorse trough over its arc-proximal facies. Thus, we speculate that King Salmon fault segments north and south of Nahlin Mountain may be two fundamentally different faults. If they are different faults, then the manner in which they have interacted with Triassic-Jurassic magmatic belts may also vary along strike.

In the Sinwa Creek area, the Whitehorse trough is most likely underlain by the Cu-Au porphyry-rich Stikine terrane, but clear evidence that the porphyry belt extends beneath the trough in the near sub-surface is currently lacking. A full accounting of the crustal level and amount of Middle Jurassic shortening across the Whitehorse Trough as well as both earlier and later translational offsets will be required before the implications for Cu-Au porphyry exploration are known.

Acknowledgments

This work was carried out under the auspices of a collaborative GSC-BCGS program delivered as a component of Geo-mapping for Energy and Minerals (GEM). Field studies were aided by the keen observations of S. Bichlmaier, S. Carroll, K. Sigloch, Y. Cui, D. Miller, and M.A. Henderson. Thanks to G. Stanley for preliminary identification of fossil corals. Isotopic analyses at the Pacific Centre for Isotopic and Geochemical Research were aided by H. Lin who did the mineral separation, and T. Ockerman who conducted activities in the clean lab, as well as C. Wall, H. Lin and N. Moerhius who all assisted with mass spectrometry. Safe, reliable and efficient helicopter support was provided by P. Vera and N. Graham of Discovery Helicopters, Atlin.

References cited

Beaudry, D., and Moore, G.F., 1981. Seismic-stratigraphic framework of the forearc basin off central Sumatra, Sunda Arc. Earth and Planetary Science Letters, 54, 17-28.

Bostock, H.S., and Lees, E.J., 1938. Laberge map-area, Yukon. Department of Mines and Resources Canada, Geological Survey of Canada, Memoir 217, 32p.

Black, L.P., Kamo, S.L., Allen, C.M., Davis, D.W., Aleinikoff, J.N., Valley, J.W., Mundil, R., Campbell, I.H., Korsh, R.J., Williams, I.S., and Foudoulis, C., 2004. Improved $^{206}Pb/^{238}U$ microprobe geochronology by monitoring of a trace-element-related matrix effect; SHRIMP, ID-TIMS, ELA-ICP-MS and oxygen isotope documentation for a series of zircon standards. Chemical Geology, 205, 115-140.

Brown, D.A., Logan, J.M., Gunning, M.H., Orchard, M.J., and Bamber, W.E., 1991. Stratigraphic evolution of the Paleozoic Stikine Assemblage in the Stikine and Iskut rivers area, northwestern British Columbia. In: Contributions to the geology and geophysics of northwestern British Columbia and southeastern Alaska, Canadian Journal of Earth Sciences 28, 958-972.

Bultman, R.B., 1979. Geology and tectonic history of the Whitehorse Trough west of Atlin, British Columbia. Unpublished Ph.D. thesis, Yale University, 284p.

Cairnes, D.D., 1910. Preliminary Memoir on the Lewes and Nordenskiold Rivers Coal District, Yukon Territory. Geological Survey of Canada, Memoir 5, 70p.

Canil, D., Mihalynuk, M., and Charnell, C., 2006. Sedimentary record for exhumation of ultrahigh pressure (UHP) rocks in the northern Cordillera, British Columbia, Canada. Geological Society of America Bulletin, 118, 1171–1184. doi: 10.1130/b2592.1.

Childe, F., and Thompson, J.F.H., 1995. U-Pb age constraints and Pb isotopic signature of the Kutcho VMS deposit; implications for the terrane affiliation of the Kutcho Formation, north central British Columbia. In: Geological Association of Canada - Mineralogical Association of Canada - Canadian Geophysical Union, Joint Annual Meeting, Program with Abstracts 20, p. 17.

Colpron, M., 2011. Geological compilation of Whitehorse trough-Whitehorse (105D), Lake Laberge (105E), and part of Carmacks (115I), Glenlyon (105L), Aishihik Lake (115H), Quiet Lake (105F) and Teslin (105C). Yukon Geological Survey, Geoscience Map, 2011-1, scale 1:250,000.

Colpron, M., and Friedman, R.M., 2007. U–Pb zircon ages for the Nordenskiöld formation (Laberge Group) and Cretaceous intrusive rocks, Whitehorse Trough, Yukon. In: Yukon Exploration and Geology 2007, 139-151.

Colpron, M., and Nelson, J.L., 2011. A Digital atlas of terranes for the northern Cordillera. British Columbia Ministry of Energy and Mines, BC Geological Survey, GeoFile 2011-11. http://www.geology.gov.yk.ca/pdf/terranes_readme.pdf accessed October 14, 2014.

Colpron, M., Crowley, J.L., Gehrels, G., Long, D.G., Murphy, D.C., Beranek, L., and Bickerton, L., 2015. Birth of the northern Cordilleran orogen, as recorded by detrital zircons in Jurassic synorogenic strata and regional exhumation in Yukon. Lithosphere, 7, 541-562.

Coney, P.J., Jones, D.L., and Monger, J.W.H., 1980. Cordilleran suspect terranes. Nature (London), 288, 329-333.

Crowley, J.L., Schoene, B., and Bowring, S.A., 2007. U-Pb dating of zircon in the Bishop Tuff at the millennial scale. Geology, 35, 1123-1126.

Currie, L.D., 1994. The geology and Mid-Jurassic amalgamation of Tracy Arm Terrane and Stikinia of northwestern British Columbia. Unpublished Ph.D. thesis, Carleton University, 385p.

Currie, L.D., and Parrish, R.R., 1997. Paleozoic and Mesozoic rocks of Stikinia exposed in northwestern British Columbia; implications for correlations in the northern Cordillera. Geological Society of America Bulletin, 109, 1402-1420.

Dickie, J.R., Grist, A.M., and Donelick, R.A., 1992. Differential uplift across the Coast plutonic complex-northern Stikine Terrane contact, Yukon; preliminary evidence from apatite fission-track thermochronometry. In: Yukon Geology, Exploration and Geological Services Division, Yukon Indian and Northern Affairs Canada, 160-166.

Dickie, J.R., and Hein, F.J., 1995. Conglomeratic fan deltas and submarine fans of the Jurassic Laberge Group, Whitehorse Trough, Yukon Territory, Canada; fore-arc sedimentation and unroofing of a volcanic island arc complex. In: Fan deltas; depositional styles and controls. Sedimentary Geology, 98, 263-292.

Dickie, J.R., and Hein, F.J., 1988. Facies and depositional setting of Laberge Conglomerates (Jurassic), Whitehorse Trough, Yukon. In: Yukon Geology, Exploration and Geological Services Division, Yukon Indian and Northern Affairs Canada, 2, 26-32.

English, J.M., Mihalynuk, M.G., Jonhnston, S.T., Orchard, M.J., Fowler, M., and Leonard, L.J., 2003. Atlin TGI, Part VI: Early to Middle Jurassic sedimentation, deformation and a preliminary assessment of hydrocarbon potential, central Whitehorse Trough and northern Cache Creek terrane. In: Geological Fieldwork 2002, British Columbia Ministry of Energy, Mines and Petroleum Resources, BC Geological Survey, Paper 2003-1, 187-201.

English, J.M., 2004. Convergent margin tectonics in the North American Cordillera: implications for continental growth and orogeny. Unpublished Ph.D. thesis, University of Victoria, Victoria, Canada, 191p.

English, J.M., Johannson, G.G., Johnston, S.T., Mihalynuk, M.G.,

Fowler, M., and Wight, K.L., 2005. Structure, stratigraphy and petroleum resource potential of the Central Whitehorse Trough, Northern Canadian Cordillera. Bulletin of Canadian Petroleum Geology, 53, 130–153. doi: 10.2113/53.2.130.

Erdmer, P., Moore, J.M., Heaman, L., Thompson, R.I., Daughtry, K.L., and Creaser, R.A., 2002. Extending the ancient margin outboard in the Canadian Cordillera: record of Proterozoic crust and Paleocene regional metamorphism in the Nicola horst, southern British Columbia. Canadian Journal of Earth Sciences, 39, 1605-1623.

Flügel, E., 2002. Triassic reef patterns. In: Phanerozoic Reef Patterns; Wolfgang. Kiessling, Erik. Flügel, and Jan. Golonka (Eds.), Society for Sedimentary Geology, Special Publication, 72, 391-463. DOI: 10.2110/pec.02.72.

Gabrielse, H., 1998. Geology of the Cry Lake and Dease Lake map areas, north-central British Columbia. Geological Survey of Canada, Bulletin 504, 147p.

Gabrielse, H., Monger, J.W.H., Wheeler, J.O., and Yorath, C.J., 1992. Tectonic framework; Part A, Morphogeological belts, tectonic assemblages and terranes. In: Geology of the Cordilleran Orogen in Canada, 15-28.

Gerstenberger, H., and Haase, G., 1997. A Highly effective emitter substance for mass spectrometric Pb isotopic ratio determinations. Chemical Geology, 136, 309-312.

Hall, R., and Smyth, H.R., 2008. Cenozoic arc processes in Indonesia: identification of the key influences on the stratigraphic record in active volcanic arcs. Geological Society of America Special Papers, 436, 27-54.

Hart, C.J.R., 1997. A transect across northern Stikinia: Geology of the northern Whitehorse map area, southern Yukon Territory (105D/13-16). Exploration and Geological Services Division, Yukon Region, Indian and Northern Affairs Canada, Bulletin, 8, 112p.

Hart, C.J.R., Dickie, J.R., Ghosh, D.K., and Armstrong, R.L., 1995. Provenance constraints for Whitehorse Trough conglomerate; U-Pb zircon dates and initial Sr ratios of granitic clasts in Jurassic Laberge Group, Yukon Territory. In: Jurassic magmatism and tectonics of the North American Cordillera, Geological Society of America, Special Paper 299, 47-63.

Hodges, M.S., and Stanley Jr, G.D., 2015. North American coral recovery after the end-Triassic mass extinction, New York Canyon, Nevada, USA. GSA Today, 25, 4-7.

Jaffey, A.H., Flynn, K.F., Glendenin, L.E., Bentley, W.C., and Essling, A.M.,1971. Precision measurement of half-lives and specific activities of ^{235}U and ^{238}U. Physical Review, C4, 1889-1906.

Johannson, G.G., 1993. Preliminary report on the stratigraphy, sedimentology, and biochronology of the Inklin Formation in the Atlin Lake area, northern British Columbia. In: Current Research, Cordillera and Pacific margin, Geological Survey of Canada, Paper 93-1A, 37-42.

Johannson, G.G., Smith, P.L., and Gordey, S.P., 1997. Early Jurassic evolution of the northern Stikinian arc; evidence from the Laberge Group, northwestern British Columbia. Canadian Journal of Earth Sciences, 34, 1030-1057.

Johnston, S.T., and Erdmer, P., 1995. Hot-side-up aureole in Southwest Yukon and limits on terrane assembly of the northern Canadian Cordillera. Geology (Boulder), 23, 419-422.

Johnston, S.T., Mortensen, J.K., and Erdmer, P., 1996. Igneous and metaigneous age constraints for the Aishihik metamorphic suite, Southwest Yukon. Canadian Journal of Earth Sciences, 33, 1543-1555.

Johnston, S.T., Mihalynuk, M.G., Brew, D.A., Hart, C.J.R., Erdmer, P., Gehrels, G.E., Currie, L.D., and Parrish, R.R., 1999. Paleozoic and Mesozoic rocks of Stikinia exposed in northwestern British Columbia; implications for correlations in the northern Cordillera; discussion and reply. Geological Society of America Bulletin, 111, 1103-1106.

Kerr, F.A., 1931a. Some of the mineral properties in the Taku District, British Columbia. Geological Survey of Canada, Summary Report 1930, Part A, 17-40.

Kerr, F.A., 1931b. Explorations between Stikine and Taku Rivers, B.C., Geological Survey of Canada, Summary Report 1930, Part A, 41-55.

Kerr, F.A., 1948. Taku River map-area, British Columbia. Geological Survey of Canada, Memoir 248, 84p.

Kreemer, C., Blewitt, G., and Klein, E.C., 2014. A geodetic plate motion and global strain rate model. Geochemistry, Geophysics, Geosystems, 15, 3849-3889.

Logan, J.M., and Mihalynuk, M.G., 2014. Tectonic controls on early Mesozoic paired alkaline porphyry deposit belts (Cu-Au ±Ag-Pt-Pd-Mo) within the Canadian Cordillera. Economic Geology, 109, 827-858.

Lowey, G.W., 2003. Preliminary lithostratigraphy of the Laberge Group (Jurassic), south-central Yukon: Implications concerning the petroleum potential of the Whitehorse Trough. Yukon Exploration and Geology, Yukon Geological Survey, 129-142.

Lowey, G.W., 2004. Sedimentology, stratigraphy and source rock potential of the Richthofen formation (Jurassic), northern Whitehorse Trough, Yukon. Yukon Exploration and Geology, Yukon Geological Survey, 177-191.

Ludwig, K.R., 2003. User's manual for Isoplot/Ex rev. 3.00: a Geochronological Toolkit for Microsoft Excel. Special Publication, 4, Berkeley Geochronology Center, Berkeley, 70p.

MacKenzie, J.M., Canil, D., Johnston, S.T., English, J., Mihalynuk, M.G., and Grant, D.B., 2005. First evidence for ultrahigh-pressure garnet peridotite in the North American Cordillera. Geology, 33, 105-108.

Mattinson, J.M., 2005. Zircon U-Pb chemical abrasion ("CA-TIMS") method: Combined annealing and multi-step partial dissolution analysis for improved precision and accuracy of zircon ages: Chemical Geology, 220, 47-66.

Mihalynuk, M.G., and Mountjoy, K.J., 1990. Geology of the Tagish Lake area (104M/ 8, 9E). In: Geological fieldwork, 1989, British Columbia Ministry of Energy, Mines and Petroleum Resources, BC Geological Survey, Paper 1990-1, 181-196.

Mihalynuk, M.G., Smith, M.T., Hancock, K.D., and Dudka, S., 1994a. Regional and economic geology of the Tulsequah River and Glacier areas (104K/12 & 13). In: Geological fieldwork 1993, British Columbia Ministry of Energy, Mines and Petroleum Resources, BC Geological Survey, Paper 1994-1, 171-197.

Mihalynuk, M.G., Smith, M.T., Hancock, K.D., Dudka, S., and Payne, J., 1994b. Geology of the Tulsequah River and Glacier areas (NTS 104K/12 & 13). British Columbia Ministry of Energy, Mines and Petroleum Resources, British Columbia Geological Survey, Open File 1994-03.

Mihalynuk, M.G., Meldrum, D., Sears, S., and Johannson, G., 1995a. Geology and mineralization of the Stuhini Creek area (104K/11). In: Geological fieldwork 1994; British Columbia Ministry of Energy, Mines and Petroleum Resources, BC Geological Survey, Paper 1995-1, 321-342.

Mihalynuk, M.G., Meldrum, D., Sears, S., Johannson, G., Madu, B.E., Vance, S., Tipper, H.W., and Monger, J.W.H., 1995b. Geology and geochemistry of the Stuhini Creek map area (NTS 104K/11). British Columbia Ministry of Energy, Mines and Petroleum Resources, British Columbia Geological Survey, Open File 1995-5.

Mihalynuk, M.G., Mountjoy, K.J., Smith, M.T., Currie, L.D., Gabites, J.E., Tipper, H.W., Orchard, M.J., Poulton, T.P., and Cordey, F., 1999. Geology and mineral resources of the Tagish Lake area (NTS 104M/ 8,9,10E, 15 and 104N/ 12W), northwestern British Columbia. British Columbia Ministry of Energy and Mines, BC Geological Survey, Bulletin 105, 201p.

Mihalynuk, M.G., Johnston, S.T., English, J.M., Cordey, F.,

Villeneuve, M.J., Rui, L., and Orchard, M.J., 2003a. Atlin TGI Part II: Regional geology and mineralization of the Nakina area (NTS 104N/2W and 3). In: Geological Fieldwork 2002, British Columbia Ministry of Energy, Mines and Petroleum Resources, BC Geological Survey, Paper 2003-1, 9-37.

Mihalynuk, M.G., Villeneuve, M.E., and Cordey, F., 2003b. Atlin TGI, Part III: Geological setting and style of mineralization at the Joss'alun occurrence, Atlin area (NTS 104N/2SW), MINFILE 104N136. In: Geological Fieldwork 2002, British Columbia Ministry of Energy, Mines and Petroleum Resources, BC Geological Survey, Paper 2003-1, 39-49.

Mihalynuk, M.G., Erdmer, P., Ghent, E.D., Cordey, F., Archibald, D.A., Friedman, R.M., and Johannson, G.G., 2004. Coherent French Range blueschist: Subduction to exhumation in < 2.5 m.y.? Geological Society of America Bulletin, 116, 910–922. doi: 10.1130/b25393.

Mihalynuk, M.G., Diakow, L.J., Friedman, R.M., and Logan, J.M., 2016. Chronology of southern Nicola arc stratigraphy and deformation. In: Geological Fieldwork 2015, British Columbia Ministry of Energy and Mines, British Columbia Geological Survey, Paper 2016-1, 31-64.

Monger, J., 1975. Upper Paleozoic rocks of the Atlin Terrane, northwestern British Columbia and south-central Yukon. Geological Survey of Canada, Paper 74-47, 63p.

Monger, J.W.H., 1977. Upper Paleozoic rocks of the western Canadian Cordillera and their bearing on Cordilleran evolution. Canadian Journal of Earth Sciences, 14, 1832-1859.

Monger, J.W.H., and Thorstad, L., 1978. Lower Mesozoic stratigraphy, Cry Lake and Spatsizi map-areas, British Columbia. In: Current research, part A., Geological Survey of Canada, Paper 78-1a, 21-24.

Mundil, R., Ludwig, K. R., Metcalfe, I., and Renne, P. R., 2004. Age and timing of the Permian Mass Extinctions: U/Pb Dating of Closed-System Zircons, Science, 305, 1760-1763.

Ootes, L., Elliott, J.M., and Rowins, S.M., 2017. Testing the relationship between the Llewellyn fault, gold mineralization, and Eocene volcanism in northwest British Columbia: A preliminary report. In: Geological Fieldwork 2016, British Columbia Ministry of Energy and Mines, British Columbia Geological Survey Paper 2017-1, this volume.

Reid, R.P., 1985. The Facies and Evolution of an Upper Triassic Reef Complex in Northern Canada (convergent Margin, Yukon, Lime Peak). Unpublished Ph.D. thesis, University of Miami, URL http://scholarlyrepository.miami.edu/dissertations/1504/ accessed December 11, 2015.

Reid, R.P., and Tempelman, K.D.J., 1987. Upper Triassic Tethyan-type reefs in the Yukon. Bulletin of Canadian Petroleum Geology, 35, 316-332.

Schiarizza, P., 2013. The Wineglass assemblage, lower Chilcotin River, south-central British Columbia: Late Permian volcanic and plutonic rocks that correlate with the Kutcho assemblage of northern British Columbia. In: Geological Fieldwork 2012, British Columbia Ministry of Energy, Mines and Natural Gas, BC Geological Survey, Paper 2013-1, 53-70.

Scoates, J.S., and Friedman, R.M., 2008. Precise age of the platinuferous Merensky Reef, Bushveld Complex, South Africa, by the U-Pb ID-TIMS chemical abrasion ID-TIMS technique, Economic Geology, 103, 465-471.

Schmitz, M.D., and Schoene, B., 2007. Derivation of isotope ratios, errors, and error correlations for U-Pb geochronology using ^{205}Pb-^{235}U-(^{233}U)-spiked isotope dilution thermal ionization mass spectrometric data. Geochemistry, Geophysics, Geosystems (G-cubed), 8, Q08006. doi:10.1029/2006GC001492.

Sigloch, K., and Mihalynuk, M.G., 2013. Intra-oceanic subduction shaped the assembly of Cordilleran North America. Nature, 496, 50-56.

Souther, J.G., 1971. Geology and mineral deposits of Tulsequah map-area, British Columbia. Geological Survey of Canada, Memoir 362, 84p.

Stacey, J.S., and Kramers, J.D., 1975. Approximation of terrestrial lead isotopic evolution by a two-stage model. Earth and Planetary Science Letters, 26, 207-221.

Stanley, G.D., 2003. The evolution of modern corals and their early history. Earth-Science Reviews, 60, 195-225.

Stern, R.A., 1997. The GSC Sensitive High Resolution Ion Microprobe (SHRIMP): analytical techniques of zircon U-Th-Pb age determinations and performance evaluation in Radiogenic age and Isotopic Studies, Report 10, Geological Survey of Canada, Current Research 1997-F, 1-31.

Stern, R.A., and Amelin, Y., 2003. Assessment of errors in SIMS zircon U-Pb geochronology using a natural zircon standard and NIST SRM 610 glass: Chemical Geology, 197, 111-142.

Tempelman-Kluit, D.J., 1984. Geology, Leberge (105E) Carmacks (115I), Yukon Territory. Geological Survey of Canada, Open File 1101, 10p. doi:10.4095/129923.

Thirlwall, M.F., 2000. Inter-laboratory and other errors in Pb isotope analyses investigated using a ^{207}Pb-^{204}Pb double spike. Chemical Geology, 163, 299-322.

Van der Werff, W., 1996. Variation in forearc basin development along the Sunda Arc, Indonesia. Journal of Southeast Asian Earth Sciences, 14, 331-349.

Vine, F.J., and Hess, H.H., 1970. Sea floor spreading. In: Maxwell, A.E. (Ed.), The Sea, Volume 4, part 2: Wiley, New York, New York, 587-622.

Wheeler, J.O., Brookfield, A.J., Gabrielse, H., Monger, J.W.H., Tipper, H.W., and Woodsworth, G.J., 1988. Terrane map of the Canadian Cordillera. Geological Survey of Canada, Map 1713A, scale 1:2,000,000, 9p.

Wheeler, J.O., 1961. Whitehorse map-area, Yukon Territory, 105D. Department of Mines and Technical Surveys, Geological Survey of Canada, Memoir 312, 156p.

Wheeler, J.O., and McFeely, P., 1991. Tectonic assemblage map of the Canadian Cordillera and adjacent parts of the United States of America. Geological Survey of Canada Map 1712A, scale 1: 2,000,000.

Wight, K.L., English, J.M., and Johnston, S.T., 2004. Structural relationship between the Laberge Group and Sinwa Formation on Copper Island, southern Atlin Lake, northwest British Columbia. In: Summary of Activities, 2004, British Columbia Ministry of Energy and Mines, Resource Development and Geoscience Branch, 113-120.

Woodsworth, G.J., Anderson, R.G., Armstrong, R.L., Struik, L.C., and van der Heyden, P., 1992. Plutonic regimes. In: Geology of the Cordilleran Orogen in Canada, 493-531.

Yarnell, J.M., Stanley, G.D., and Hart, C.J., 1998. New paleontological investigations of Upper Triassic shallow-water reef carbonates (Lewes River Group) in the Whitehorse area, Yukon. In: Yukon Exploration and Geology 1998, Exploration and Geological Services Division, Yukon, Indian and Northern Affairs Canada, 179-184.

Zagorevski, A., Mihalynuk, M.G., Joyce, N., Kellett, D.A., and Milidragovic, D., 2015. Characterization of volcanic and intrusive rocks across the British Columbia – Yukon border, GEM 2 Cordillera. Geological Survey of Canada, Open File 7956, 13p. doi:10.4095/297272.